JOURNAL OF PETROLOGY | VOLUME 0 | NUMBER 0 | PAGES 1–27 | 2013 | doi:10.1093/petrology/egt017
Journal of Petrology Advance Access published April 23, 2013

The Demir Kapija Ophiolite, Macedonia (FYROM): a Snapshot of Subduction Initiation within a Back-arc

MILICA BOŽOVIĆ[1], DEJAN PRELEVIĆ[1]*, ROLF L. ROMER[2], MATTHIAS BARTH[1], PAUL VAN DEN BOGAARD[3] AND BLAŽO BOEV[4]

[1]JOHANNES GUTENBERG-UNIVERSITÄT, INSTITUT FÜR GEOWISSENSCHAFTEN, FB 09, MINERALOGIE, BECHERWEG 21, 55099 MAINZ, GERMANY

[2]HELMHOLTZ CENTRE POTSDAM, GFZ GERMAN RESEARCH CENTRE FOR GEOSCIENCES, SECTION 4.2, INORGANIC AND ISOTOPE GEOCHEMISTRY, TELEGRAFENBERG, B 126, D-14473 POTSDAM, GERMANY

[3]LEIBNIZ-INSTITUT FÜR MEERESWISSENSCHAFTEN, IFM-GEOMAR, WISCHHOFSTR. 1–3, 24148 KIEL, GERMANY

[4]GOCE DELČEV FACULTY, KRSTE MISIRKOV BB, 2000 ŠTIP, FYRO MACEDONIA

RECEIVED OCTOBER 24, 2011; ACCEPTED MARCH 1, 2013

The Demir Kapija ophiolitic complex in southern Macedonia–FYROM (Former Yugoslav Republic of Macedonia) represents the southernmost exposure of the Tethyan Eastern Vardar ophiolitic unit in the Eastern Mediterranean. It consists of a mafic volcanic sequence (pillow basalts, sheeted dyke diabases and gabbros) that was subsequently intruded by island arc magmas with and without adakitic affinity. The mafic volcanic sequence is characterized by slightly increased ratios of large ion lithophile elements to high field strength elements (LILE/HFSE), flat rare earth element (REE) patterns, radiogenic $^{143}Nd/^{144}Nd$ (up to 0·51272) and high TiO_2 contents (which reflect Pl + Ol + Cpx fractionation). The relationship between TiO_2 and MgO contents indicates that Ti saturation was eventually reached and that Ti-magnetite fractionated. The mafic volcanic sequence of the ophiolite complex formed around 166·4 Ma in a short-lived intra-oceanic back-arc basin by slab rollback of the Western Vardar Ocean. The rocks with and without adakitic affinity are spatially and temporally closely related. Their crystallization age is around 164 Ma. Our data suggest that two subgroups of arc lavas evolved as discrete volcanic lineages that are not related by fractional crystallization of a common parental magma, and that two different parental magmas are required. The arc lavas with adakitic affinity show some of the typical features of adakites; that is, low heavy REE, elevated Sr/Y, high LILE and high light REE. Major and trace element compositions of clinopyroxene phenocrysts resemble those of typical adakite-derived clinopyroxene. The very high Th/La, Th/Yb and Ba/Yb ratios and the reduced $^{143}Nd/^{144}Nd$ values (around 0·51245) of the rocks with adakitic affinity are considered to reflect contributions of sedimentary material to their mantle source. By analogy with adakites, these rocks are interpreted as the product of slab + sediment melting in an unusually hot subduction zone (subduction of young oceanic crust). In contrast, the arc lavas without adakitic affinity are related to a different parental melt, similar to common arc magmas. The Demir Kapija ophiolite formed in a short-lived intra-oceanic back-arc basin during subduction initiation within a back-arc. The arc intrusions are related to the change from an extensional to a compressional regime.

KEY WORDS: *ophiolite; back-arc; MORB; intra-oceanic subduction; adakite-like rock; ridge collapse*

INTRODUCTION

Since the late 1970s, it has been increasingly recognized that the petrology and geochemistry of ophiolites predominantly resemble those of lithological units from intra-oceanic subduction zones, ranging from nascent- and fore- to intra- or back-arcs, ruling out analogy with modern oceanic ridge lithosphere. This conclusion is

*Corresponding author. E-mail: prelevic@uni-mainz.de

largely based on studies of the Troodos and Oman ophiolites, which have revealed that the mafic members have geochemical characteristics transitional between those of mid-ocean ridge basalts (MORB) and island arc tholeiites (IAT). These ophiolites have a close spatial and temporal relationship with supra-subduction zone volcanic rocks found exclusively in intra-oceanic, fore-arc systems (e.g. Pearce & Cann, 1973; Pearce *et al.*, 1984; Crawford *et al.*, 1989; Ishikawa *et al.*, 2005; Saccani *et al.*, 2011), or related to subduction initiation (Stern & Bloomer, 1992).

Recent studies in the Izu–Bonin–Mariana (IBM) arc have improved understanding of subduction initiation and the subsequent development of fore-arc stratigraphy (Reagan *et al.*, 2010; Ishizuka *et al.*, 2011). The typical stratigraphic succession of the IBM includes mantle peridotite, gabbros, a sheeted dyke complex, pillow basalts and finally boninites, high-magnesian andesites, tholeiites and calc-alkaline arc lavas. This fore-arc stratigraphy is remarkably similar to that observed in Tethyan ophiolites, implying that the fore-arc crustal section that is produced during subduction initiation, and preserved in the IBM system, represents an *in situ* section of a future supra-subduction zone ophiolite (Reagan *et al.*, 2010; Ishizuka *et al.*, 2011). Recently, Whattam & Stern (2011) recognized that magmatic progression from less to more high field strength element (HFSE)-depleted and large ion lithophile element (LILE)-enriched compositions within bimodal ophiolitic sequences, represents the major diagnostic feature for a subduction initiation origin of the ophiolite complex.

There are several Mesozoic ophiolite belts in the Balkan area (Fig. 1). The Demir Kapija ophiolite (FYROM) and Guevgelia block (Greece) represent the southernmost exposures of the Eastern Vardar Ophiolitic Unit, which is separated from the Western Vardar Ocean(s) by the Sava zone. This large remnant of Tethyan oceanic lithosphere can be traced from the South Apuseni Mountains in the north, through the southern Pannonian Basin, Serbia, Macedonia–FYROM (Demir Kapija ophiolite) and Greece (Guevgelia block) to Turkey in the SE (Fig. 1). The Demir Kapija ophiolite comprises well-exposed sections of oceanic crust with gabbro–sheeted dyke diabases–pillow basalts (Fig. 2), intruded by arc rocks.

In this study we present whole-rock major and trace element and Sr, Nd and Pb isotope data, as well as clinopyroxene trace element data for the Demir Kapija ophiolite slice. Our data, together with new age data, are used to constrain both the genesis of the arc volcanic rocks that intrude the sheeted dyke complex and their relation to the geotectonic evolution of the Tethyan ocean. Compared with normal island arcs, our data imply that exceptionally high amounts of melt derived from subducting sediments play a role in the origin of the arc rocks, making the Demir Kapija ophiolite a unique Tethyan ophiolitic assemblage. We propose a new model for the formation and closure of the Demir Kapija basin, connecting the ophiolite origin with back-arc spreading ridge collapse and subsequent subduction initiation within a marginal ocean basin. It is this special geotectonic setting that eventually allowed melting of an exceptionally young oceanic slab and overlying terrigeneous sediments at the transition between amphibolite- and eclogite-facies conditions.

GEOLOGY OF MACEDONIAN (FYROM) OPHIOLITES

The crust of Macedonia (FYROM) comprises several tectonic units that extend to the northern and southern Balkans. The western part of Macedonia belongs to the Dinarides–Hellenides belt. It is thought to have formed by collision between the continental margins of Adria and Eurasia (Pamić *et al.*, 2002; Bortolotti & Principi, 2005; Zelić *et al.*, 2010). The central part of Macedonia includes two units: the Pelagonides and the Vardar Zone. The Pelagonides are a moderate- to high-grade metamorphic terrane of Precambrian rocks that extends northward from the Skutari–Peć line to the Drina–Ivanjica metamorphic terrane (Marović *et al.*, 2000; Lepitkova, 2002; Anders *et al.*, 2006; Karamata, 2006; Schmid *et al.*, 2008; Robertson *et al.*, 2009). The Pelagonides represent a thrust sheet from the distal part of the Adriatic passive margin (Schmid *et al.*, 2008). The Vardar Zone of central Macedonia comprises the Western Vardar Ophiolitic Unit (*sensu* Schmid *et al.*, 2008) or Dinaric ophiolitic unit (*sensu* Karamata, 2006) and the Eastern Vardar Ophiolitic Unit. The Eastern Vardar ophiolite crops out in the SE part of Macedonia, where it forms the ophiolitic complex of Demir Kapija (Fig. 2). The Eastern Vardar ophiolite represents a geotectonic entity distinct from the Dinaride ophiolite belt and the Western Vardar ophiolite (Karamata, 2006; Schmid *et al.*, 2008).

The easternmost part of Macedonia belongs to the Serbian–Macedonian massif (Fig. 1 inset), extending from eastern Serbia to northern Greece (Fig. 1 inset). This crystalline terrane comprises high- to medium-grade metamorphic units that were separated from Gondwana during a Triassic rifting episode that led to the formation of a branch of the Neotethys Ocean (Vardar–Meliata Ocean) (Balogh *et al.*, 1994; Himmerkus *et al.*, 2002, 2009*a*, 2009*b*; Meinhold *et al.*, 2010). They are of both MORB and subduction-related affinity (Balogh *et al.*, 1994). Rb/Sr and K/Ar age data suggest metamorphism during a Palaeozoic orogeny (488 ± 19 Ma), with Variscan and younger metamorphic overprints at ~275 and 160–127 Ma, respectively (Balogh *et al.*, 1994).

The NW–SE-aligned, dismembered, ophiolitic complex of Demir Kapija is around 50 km long and 25 km wide (Fig. 2). The 'volcanic' sequence comprises pillow basalts, a diabase sheeted dyke complex and gabbros, intruded by

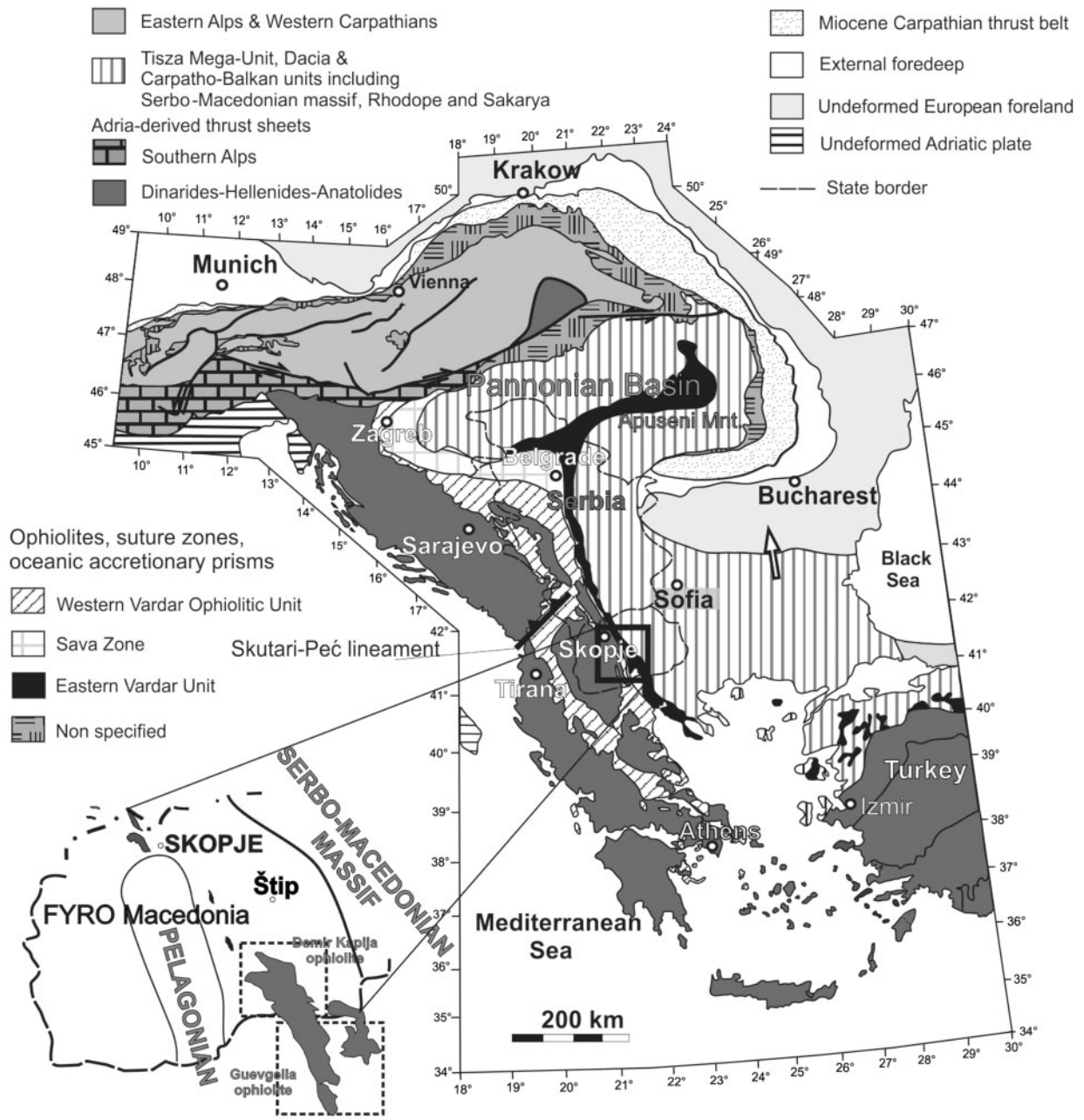

Fig. 1. Map showing the location of the study area in the context of the major tectonic units of the Alps, Carpathians, Dinarides and Hellenides [simplified after Schmid *et al.* (2008) and Ustaszewski *et al.* (2009)].

subduction-related volcanic rocks. Small serpentinized peridotite occurrences include mostly chromite-bearing dunite with minor wehrlite and lherzolite (Supplementary Data 1, available for downloading at http://www.petrology.oxfordjournals.org). Granodiorites and granites extend from Štip, Konečke Mt. and Plauš to Furka (Fanos in Greece) (Fig. 2). They are considered to have been generated during a post-collisional episode shortly after the Jurassic collisional events responsible for ophiolite emplacement (Šarić *et al.*, 2009). The whole ophiolitic section is overlain by basal conglomerates containing pebbles of subduction-related volcanic rocks, which are overlain by Upper Tithonian reef limestones (Supplementary Data 1). In the NW and SE, the limestones are covered by upper Eocene–Pliocene and Pliocene–Quaternary sediments, respectively. In the west, the Demir Kapija complex is in tectonic contact with the Pelagonian metamorphic complex, whereas the north-eastern tectonic contact with the Serbo-Macedonian massif

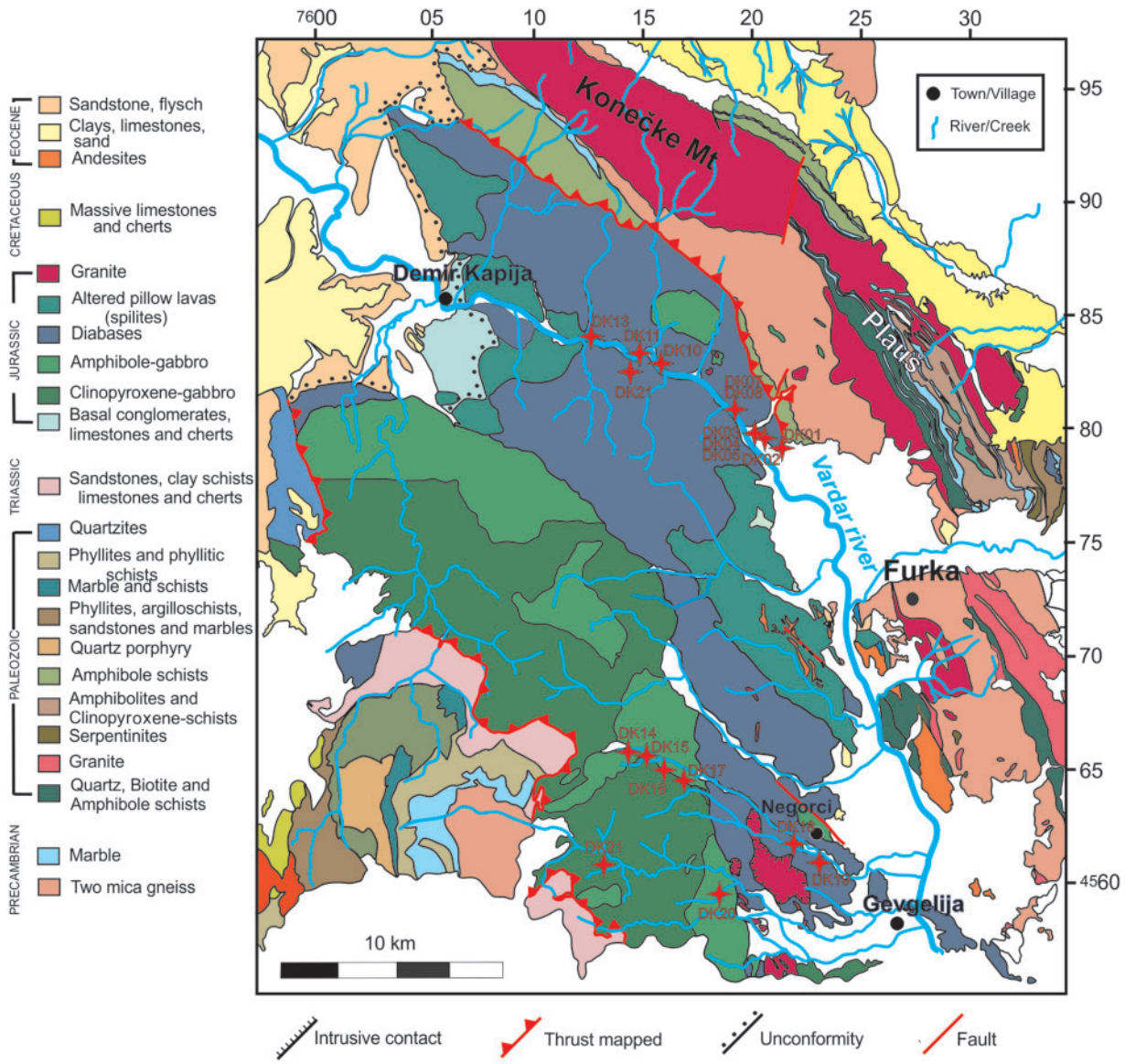

Fig. 2. Simplified geological map of the study area, redrawn and modified from Geological Institute of Yugoslavia basic geological map, sheets Gevgelija, Kavadarci, Kozuf and Strumica; 1:100 000.

is characterized by a mylonite zone and tectonic mélange (Lepitkova, 2002; Supplementary Data 1).

SAMPLE SELECTION

The following igneous rocks of the Demir Kapija ophiolite were investigated: (1) gabbros, (2) sheeted dyke diabases and pillow basalts; (3) subduction-related magmatic rocks that intrude the sheeted dyke complex and gabbros.

Field relations and petrography

Gabbros are fine- to medium-grained clinopyroxene gabbros and rare olivine gabbros, troctolites, and amphibole gabbros. Clinopyroxene gabbros consist of plagioclase and clinopyroxene with rare secondary amphibole and magnetite. Olivine gabbros range from troctolites to clinopyroxene gabbros with olivine. Amphibole gabbros are usually found in tectonic zones and formed by alteration of rocks of the other gabbro types. Secondary minerals include magnetite, titanite, quartz, biotite, epidote, zoisite and chlorite.

Diabases of the sheeted dike complex represent the dominant lithology in the Demir Kapija ophiolite. Dikes show symmetric or asymmetric chilled margins against adjacent dikes. The rocks consist of euhedral plagioclase laths enclosed by anhedral to subhedral clinopyroxene. In many cases alteration under greenschist-facies conditions has left only relicts of the original mineral assemblage.

Magnetite is commonly found as an accessory phase and is locally very abundant (up to 20 vol. %). Plagioclase is altered to sericite or albite ± zeolite minerals, whereas clinopyroxene is often transformed to tremolite/actinolite group amphiboles and chlorite. Epidote and calcite are also present. Glass is completely transformed to chlorite and/or epidote.

Pillow basalts form units of variable thickness from a few metres to a few tens of metres (Fig. 3a). These have an intersertal texture with 0·5 mm plagioclase laths in an original glassy matrix, which is now transformed to chlorite and zeolite minerals.

The gabbros, sheeted dike diabases and pillow basalts are intruded by subduction-related magmatic rocks that occur as dikes, plugs or small sills (Fig. 3a, b, d and e). Based on the geochemical data shown below, magmatic rocks with and without adakitic affinity may be distinguished. The thickness of the dikes never exceeds 5 m whereas domal intrusions are up to 20 m wide and less than 10 m high. In the dome-like occurrences, fine-grained enclaves, sometimes almost completely fragmented, occur along the contact with more felsic, coarse-grained, reddish host rocks, and vice versa (Fig. 3e). Both rock types have lobate mutual contacts indicating that they were at least partially molten at the time of intrusion. The presence of enclaves of adakitic affinity within magmatic rocks without adakitic affinity (and vice versa) represents first-order evidence for a mingling–mixing relationship (Fig. 3c).

The subduction-related rocks are porphyric: those without adakitic affinity consist of plagioclase plus mafic minerals (amphibole), whereas those with adakitic affinity consist of plagioclase plus clinopyroxene. The nature of the mafic minerals in rocks without adakitic affinity is largely obliterated owing to alteration to chlorite and tremolite/actinolite–epidote. Plagioclase is often transformed to albite and can be as large as 2 mm in some samples.

Sampling strategy

In the course of this study, more than 60 samples were collected. Global positioning system (GPS) coordinates of the sampled localities are given in Supplementary Data 2. Samples were studied first petrographically before selecting the freshest samples for powdering. From this collection we selected 49 samples for whole-rock chemical analysis, representing more than 20 dykes, sills and gabbro bodies. All 49 samples were analysed for major and trace elements. A subset of 20 selected samples was analysed for their Sr, Nd and Pb isotope composition. The samples used for isotope analysis were leached before their isotopic compositions were determined. Whole-rock, major and trace element compositions of representative samples from both groups are reported in Table 1. Their Sr, Nd, and Pb isotopic compositions are given in Table 2. The full dataset is available as Supplementary Data 3.

ANALYTICAL METHODS

Whole-rock major elements were determined by X-ray fluorescence (XRF) spectrometry using a Philips MagiXPRO spectrometer on fused discs at the University of Mainz. Trace elements for all rock powders were analyzed by laser ablation inductively coupled plasma mass spectrometry (LA-ICP-MS) using an Agilent 7500ce ICP-MS system coupled with a New Wave UP-213 LA system at the University of Mainz. Rock powders were melted to form glass beads, without any flux agent, on an iridium strip heater in an argon atmosphere and analyzed by laser sampling of the glass (Nehring *et al.*, 2008).

Powders used for isotopic analysis were leached in 6N HCl overnight before being digested using HF in closed screw-top Savillex beakers on a hotplate for 4 days. This leaching should preferentially remove any secondary minerals and, thus, the isotope signature associated with them. Solutions were evaporated to near dryness, taken up in HNO_3 to convert fluorides to nitrates and slowly dried again. The samples were redissolved in 6N HCl and once a clear solution was obtained split for Sr–Nd and Pb isotope analysis. Sr, Nd, and Pb were separated using standard ion-exchange procedures (Romer *et al.*, 2001, 2005). Special care was taken to remove Ba from the REE fraction (using an additional washing step with 2·5N HNO_3) to avoid interferences of BaO on mass ^{146}Nd. Sr and Nd isotope compositions were measured on VG 54-30 Sector (Ta single filaments) and Finnigan MAT 262 (Re double filaments) thermal ionization multi-collector mass spectrometers, respectively, both operated in dynamic multi-collection mode (Deutsches GeoForschungs Zentrum, Potsdam, Germany). During the measurement period, NBS-987 Sr-reference material and the La Jolla Nd-standard yielded average $^{87}Sr/^{86}Sr$ and $^{143}Nd/^{144}Nd$ values of 0·710270 ± 14 (2σ of 18 measurements) and 0·511850 ± 7 (2σ of 11 measurements), respectively. The Pb isotopic composition was measured on a Finnigan MAT 262 instrument on single Re filaments using static multi-collection (Deutsches GeoForschungsZentrum, Potsdam, Germany). Instrumental fractionation was corrected with 0·1% per a.m.u. as determined from the long-term reproducibility of Pb reference material NBS-981. Accuracy and precision of reported Pb isotope ratios is better than 0·1% at the 2σ level of uncertainty. Trace element contents used for the calculation of the initial isotopic values are combined LA-ICP-MS and XRF data for the unleached powders.

The major element composition of minerals was determined by electron microprobe (JEOL JXA 8900RL) at the Department of Geosciences, University of Mainz, Germany, using wavelength-dispersive analysis and a range of natural and synthetic standards. The data were corrected using the CITZAF procedure (Armstrong, 1995); detection limits were between 0·01 and 0·07 wt %.

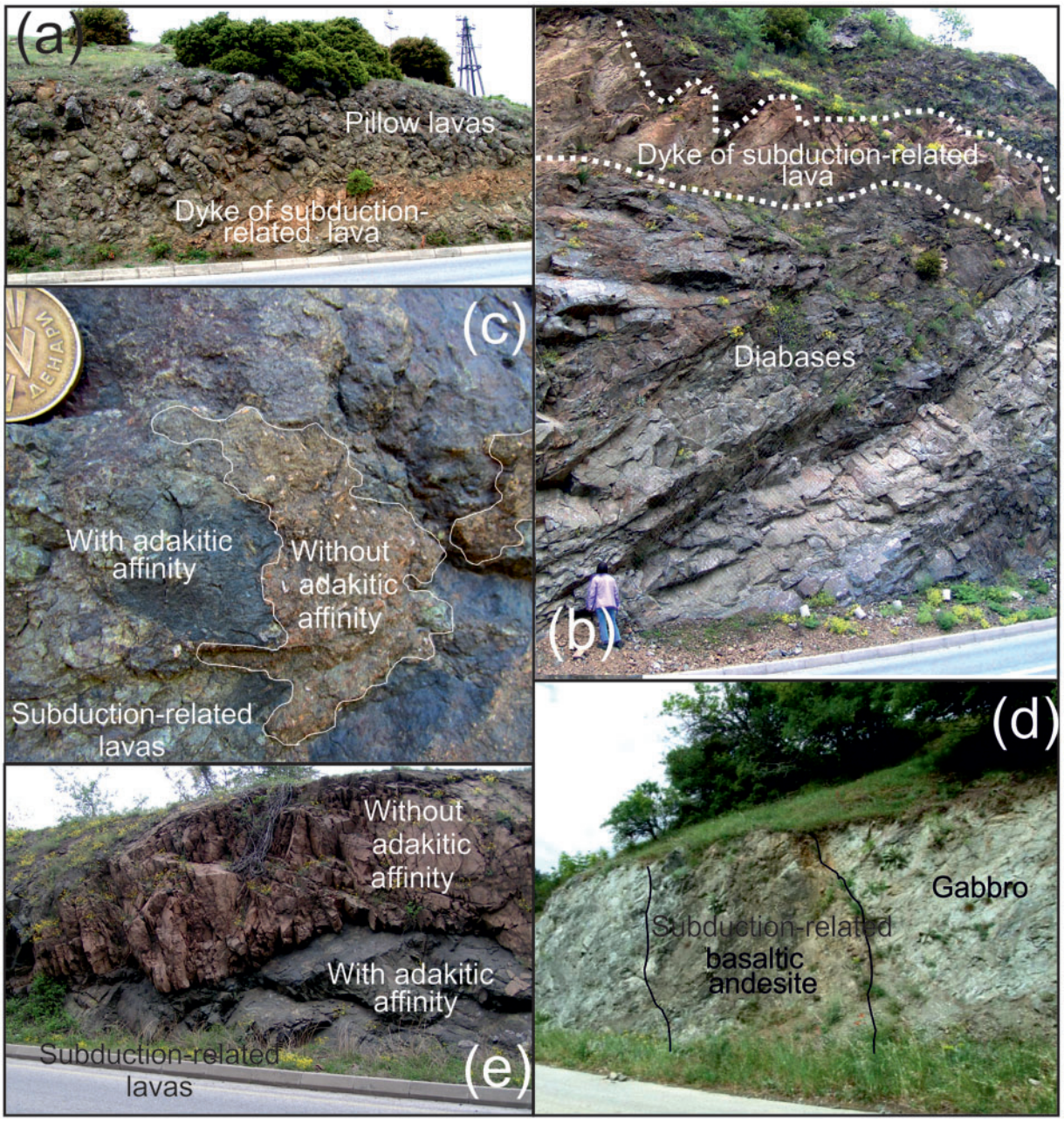

Fig. 3. Field photographs. (a) A dyke of subduction-related rock without adakitic affinity intruding pillow basalts. (b) Sheeted dyke rocks represented by pale gray diabases intruded by subduction-related rock without adakitic affinity (reddish yellow). (c) A close-up of a dome-like intrusion showing fine-grained enclaves and blobs of a felsic rock without adakitic affinity within a more mafic host-rock with adakitic affinity. (Note the lobate contacts indicating that both rock types were at least partially molten at the time of intrusion.) (d) Over-step sequence represented by basal conglomerates with pebbles of rocks with and without adakitic affinity and chert. (e) A dome-like intrusion of reddish felsic rock without adakitic affinity surrounding more mafic rock with adakitic affinity.

Operating conditions were generally 15 kV (20 kV) accelerating voltage, 12 nA beam current, 1–5 μm beam diameter and 15–30 s counting time on peak. Synthetic and natural minerals were used for standardization.

Mineral trace element compositions were determined *in situ*, by LA-ICP-MS at the University of Mainz, Germany. The laser was operated at a repetition rate of 10 Hz and laser energy densities of ~6·5 J cm^{-2}, using helium as carrier gas. All measurements were performed on polished thin sections of 100 μm thickness with spot diameters of 30–50 μm. Data collection was monitored in time-resolved format and the data were processed on-line using

Table 1: Representative major (wt %) and trace element (ppm) analyses of Demir Kapija igneous rocks

	Diabases and pillow basalts				Subduction related, without adakitic affinity					Gabbro
Sample:	06DK09	06DK19	06DK25	09DK31	06DK03	06DK07	06DK11	06DK13	06DK16	GBR
SiO_2	49·7	50·2	58·0	49·9	42·9	62·3	72·7	52·2	67·6	47·7
TiO_2	2·56	1·81	1·54	1·17	0·70	0·52	0·40	2·19	0·4	0·16
Al_2O_3	13·0	14·4	14·6	15·8	12·3	14·5	13·7	13·4	13·7	13·5
Fe_2O_3	14·9	13·2	10·8	10·3	6·92	5·61	3·7	13·46	3·2	5·86
MnO	0·23	0·19	0·15	0·2	0·13	0·11	0·06	0·16	0·09	0·11
MgO	4·95	6·93	2·79	6·18	6·18	2·49	0·77	5·2	0·93	14·9
CaO	4·27	4·79	3·52	8·13	14·1	3·1	0·98	7·07	4·27	16·4
Na_2O	4·51	5·37	7·06	4·75	5·4	4·88	5·54	5·34	2·32	0·56
K_2O	0·15	0·30	0·74	0·13	0·06	2·78	2·37	0·44	3·21	0·01
P_2O_5	0·26	0·16	0·27	0·17	0·08	0·10	0·06	0·21	0·07	n.d.
LOI	5·84	3·9	2·07	4·16	12·03	4·16	1·2	1·73	5·52	0·64
Sum	100·3	101·2	101·5	100·9	100·9	100·5	101·5	101·5	101·3	100·1
V	*480*	*407*	*222*	*291*	n.m.	*111*	*8·26*	*465*	*23·4*	*232*
Cr	*6·49*	*16·3*	*6·88*	*6·91*	n.m.	*51·7*	n.m.	*33·1*	*2·04*	*52·5*
Ni	*26·9*	*25·5*	*13·1*	*20·4*	n.m.	*24·7*	*0·35*	*26·4*	*1·30*	*54·7*
Rb	2·33	6·88	9·75	2·69	0·450	78·0	44·8	9·65	99·5	16·1
Sr	55·21	98·0	71·1	173	110	134	40·9	179	50·2	267
Y	46·6	28·6	64·6	28·0	16·2	27·1	32·1	45·4	28·1	14·2
Zr	150	93·4	243	88·6	43·6	121	184	93·9	144	98·1
Nb	6·29	2·70	9·92	1·55	1·17	4·56	5·73	5·20	4·71	2·86
Ba	18·2	22·6	61·7	26·9	23·4	538	423	40·9	104	206
La	7·85	2·39	14·0	10·0	4·58	21·7	10·8	6·01	26·8	34·9
Ce	21·8	8·05	38·5	24·62	10·3	49·7	31·2	17·3	57·3	71·10
Pr	3·33	1·33	5·32	3·42	1·51	5·71	3·74	2·91	6·66	8·03
Nd	17·7	8·30	27·1	17·0	7·29	24·1	17·0	15·1	27·4	31·8
Sm	5·76	3·14	7·75	4·68	1·94	5·29	4·23	5·02	5·93	6·31
Eu	1·87	1·16	2·22	1·64	0·727	1·33	1·08	1·61	1·35	1·45
Gd	7·45	4·00	9·82	5·15	2·48	5·02	4·71	6·60	4·92	4·36
Tb	1·251	0·708	1·62	n.m.	0·412	0·737	n.m.	1·164	n.m.	n.m.
Dy	8·73	5·31	11·9	5·38	3·00	4·89	6·32	8·19	5·04	3·23
Ho	1·73	1·09	2·36	1·10	0·592	1·03	1·45	1·64	1·02	0·595
Er	5·26	3·13	7·02	3·09	1·76	3·06	4·61	5·00	3·10	1·71
Tm	0·723	0·477	1·06	n.m.	0·258	0·452	n.m.	0·725	n.m.	n.m.
Yb	5·39	3·53	7·64	2·97	1·84	3·26	4·73	5·02	3·24	1·50
Lu	0·756	0·491	1·11	0·436	0·268	0·480	0·768	0·698	0·493	0·218
Hf	4·33	2·52	6·32	2·30	1·32	3·45	6·06	3·05	3·75	3·13
Ta	0·580	0·215	0·791	0·108	0·127	0·639	0·569	0·523	0·820	0·206
Pb	*6*	*6*	*7*	*3*	*3*	*7*	*9*	n.d.	*6*	*3*
Th	0·823	n.d.	1·61	1·55	n.d.	9·70	9·89	2·90	15·2	22·1
U	0·231	n.d.	0·629	0·531	n.d.	2·69	2·39	n.d.	4·14	3·38

(continued)

Table 1: Continued

	Subduction related, without adakitic affinity							Subduction related, with adakitic affinity		
Sample:	06DK02a	10DK49f	10DK61	10DK62	10DK63	10DK68d	10DK68l	09DK34	06DK10	09DK29
SiO_2	51·7	47·0	49·1	49·9	62·2	53·5	70·9	50·4	50·6	49·0
TiO_2	0·79	0·72	0·78	0·34	0·34	0·9	0·34	0·71	0·73	0·67
Al_2O_3	16·0	14·8	16·2	13·7	12	15·2	11·9	16·2	15·9	16·5
Fe_2O_3	8·95	9·49	8·46	2·78	2·52	7·8	2·69	7·76	8·21	8·67
MnO	0·15	0·15	0·19	0·05	0·03	0·15	0·07	0·18	0·18	0·17
MgO	4·66	12	5·10	0·82	0·40	3·29	0·98	6·4	5·73	7·35
CaO	4·63	10·6	6·61	11·1	7·99	5·61	2·93	9·3	9·10	8·75
Na_2O	5·55	1·75	3·74	1·81	3·28	2·51	1·67	4·3	5·15	3·04
K_2O	2·51	0·06	1·77	7·64	3·76	2·82	4·25	0·78	0·53	1·6
P_2O_5	0·12	0·08	0·12	0·08	0·07	0·24	0·06	0·2	0·19	0·17
LOI	5·57	3·7	8·24	10·58	7·42	8·52	4·54	3·75	4·22	4·22
Sum	100·6	100·5	100·4	98·8	99·9	100·5	100·3	100·0	100·5	100·1
V	*329*	n.m.	n.m.	n.m.	n.m.	n.m.	n.m.	*231*	*268*	*195*
Cr	*2·51*	*1786*	*23·1*	*3·21*	*3·99*	*18·8*	*4·81*	*52·5*	*26·4*	*39·7*
Ni	*11·5*	*341*	*30·2*	*5·47*	*5·04*	*4·89*	*7·06*	*54·7*	*49·4*	*64·8*
Rb	50·3	0·788	59·0	108	82·0	78·2	88·7	16·1	17·5	82·5
Sr	161	188	239	138	145	65·5	65·3	267	314	459
Y	18·1	14·7	16·6	24·9	24·5	27·7	23·4	14·2	16·4	10·9
Zr	77·3	46·1	88·4	151	174	115	134	98·0	120	93·6
Nb	3·07	1·52	4·97	13·9	10·2	4·72	5·63	2·86	3·34	2·34
Ba	321	48·8	521	604	349	263	536	206	159	727
La	13·5	5·46	18·4	26·1	25·4	19·6	20·4	34·8	33·2	21·2
Ce	30·9	14·44	37·62	46·81	52·73	43·02	47·73	71·1	71·5	47·7
Pr	3·63	1·83	4·43	4·86	6·11	5·15	5·21	8·03	8·72	5·63
Nd	15·6	8·68	19·1	19·0	25·0	22·2	21·1	31·8	33·7	22·9
Sm	3·46	2·30	4·12	3·74	5·08	5·29	4·56	6·31	5·90	3·90
Eu	1·05	0·752	1·08	0·903	0·986	1·35	1·00	1·45	1·49	0·944
Gd	3·49	2·45	3·48	3·42	4·48	5·13	3·98	4·36	4·49	3·22
Tb	0·488	n.m.	n.m.	n.m.	n.m.	n.m.	n.m.	n.m.	0·538	n.m.
Dy	3·29	2·74	3·13	4·00	4·42	5·05	4·07	3·23	3·29	2·48
Ho	0·666	0·569	0·630	0·816	0·912	1·01	0·821	0·600	0·597	0·472
Er	1·93	1·66	1·78	2·50	2·71	2·83	2·58	1·71	1·68	1·27
Tm	0·294	n.m.	n.m.	n.m.	n.m.	n.m.	n.m.	n.m.	0·208	n.m.
Yb	2·07	1·65	1·84	2·60	2·73	2·68	2·62	1·50	1·62	1·23
Lu	0·284	0·244	0·259	0·388	0·415	0·390	0·394	0·220	0·228	0·191
Hf	2·16	1·28	2·43	3·89	4·59	3·14	3·49	3·13	3·33	2·37
Ta	0·369	0·115	0·531	1·25	0·880	0·403	0·461	0·210	0·393	0·152
Pb	*15*	*1*	*52*	*61*	*57*	*17*	*0·4*	3·38	*8*	*4*
Th	6·29	1·61	5·47	22·2	22·3	9·96	10·9	22·1	24·0	20·2
U	1·71	0·662	3·30	7·52	5·68	2·56	3·21	3·38	3·92	2·41

The locations for each analysed sample are presented in Supplementary Data 2. Italic type indicates XRF analyses. n.d., not detected. n.m., not measured.

Table 2: Whole-rock Sr, Nd, and Pb isotope data for the Demir Kapija igneous rocks

Sample	$^{87}Sr/^{86}Sr$*	$^{87}Sr_{(T)}/^{86}Sr$†	$^{143}Nd/^{144}Nd$*	$^{143}Nd_{(T)}/^{144}Nd$†	$^{206}Pb/^{204}Pb$‡	$^{207}Pb/^{204}Pb$‡	$^{208}Pb/^{204}Pb$‡	$^{206}Pb/^{204}Pb$§	$^{207}Pb/^{204}Pb$§	$^{208}Pb/^{204}Pb$§
06DK02a	0·707637 ± 5	0·70603	0·512669 ± 10	0·51255	19·506	15·669	39·439	17·05	15·57	39·26
06DK03	0·705356 ± 5	0·70533	0·512890 ± 9	0·51270	18·794	15·661	38·906	18·79	15·66	38·91
06DK07	0·709183 ± 3	0·70607	0·512722 ± 3	0·51257	19·575	15·722	39·508	18·95	15·69	38·92
06DK09	0·705459 ± 8	0·70518	0·512965 ± 5	0·51275						
06DK10	0·705950 ± 7	0·70558	0·512495 ± 5	0·51237	19·508	15·705	40·672	18·87	15·67	39·39
06DK11	0·711472 ± 7	0·70320	0·512707 ± 5	0·51251	19·760	15·712	39·679	18·76	15·66	38·89
06DK13	0·705027 ± 7	0·70462	0·512919 ± 7	0·51272	19·312	15·670	39·956	19·03	15·66	38·49
06DK16	0·705270 ± 4	0·70487	0·512773 ± 5	0·51264	20·669	15·813	40·564	19·51	15·76	39·34
06DK19	0·729735 ± 4	0·71647	0·512936 ± 6	0·51268	18·653	15·648	38·826	18·65	15·65	38·83
06DK25	0·705063 ± 6	0·70433	0·512944 ± 6	0·51275	19·555	15·598	39·610	19·53	15·59	39·55
09DK29	0·706643 ± 5	0·70536	0·512511 ± 5	0·51239	19·599	15·712	40·894	18·51	15·66	37·91
09DK31	0·705227 ± 6	0·70513	0·512807 ± 6	0·51262	18·807	15·667	38·984	18·50	15·65	38·66
09DK34	0·703070 ± 10	0·70306	0·512482 ± 11	0·51237	19·544	15·743	40·932	17·82	15·66	37·28
GBR	0·706070 ± 3	0·70567	0·513111 ± 17	0·51276	17·840	15·566	37·678	17·77	15·56	37·61
10DK49f	0·704722 ± 3	0·70469	0·512743 ± 5	0·51256	18·828	15·660	39·163	17·86	15·61	38·39
10DK61	0·706659 ± 6	0·70503	0·512728 ± 6	0·51258	18·880	15·669	38·765	18·77	15·66	38·71
10DK62	0·708289 ± 4	0·70314	0·512700 ± 6	0·51257	18·883	15·666	39·007	18·68	15·66	38·81
10DK63	0·708050 ± 3	0·70434	0·512598 ± 5	0·51246	19·164	15·692	39·164	18·99	15·68	38·95
10DK68d	0·711498 ± 6	0·70364	0·512691 ± 13	0·51253	18·817	15·663	38·899	18·57	15·65	38·58
10DK68h	0·714930 ± 3	0·70599	0·512694 ± 7	0·51255						

*$^{87}Sr/^{86}Sr$ and $^{143}Nd/^{144}Nd$, normalized to $^{86}Sr/^{88}Sr = 0{\cdot}1194$ and $^{146}Nd/^{144}Nd = 0{\cdot}7219$, respectively. Analytical uncertainties are given at $2\sigma_m$ level.
†$^{87}Sr/^{86}Sr_{(T)}$ and $\varepsilon Nd_{(T)}$ were age corrected on 160 Ma, using $\lambda^{87}Rb = 1{\cdot}42E - 11\ a^{-1}$ and $\lambda^{147}Sm = 6{\cdot}54E - 12\ a^{-1}$, $(^{147}Sm/^{144}Nd)^0_{CHUR} = 0{\cdot}1967$, and $(^{143}Nd/^{144}Nd)^0_{CHUR} = 0{\cdot}512638$, respectively, and the concentration data given in Table 1.
‡Lead isotope data corrected for mass discrimination with 0·1% per a.m.u. Reproducibility at 2σ level is better than 0·1%.
§Lead isotope data age corrected on 160 Ma using the contents of Pb, Th, and U (Table 1) and the constants recommended by IUGS ($\lambda^{232}Th = 4{\cdot}9475E - 11\ a^{-1}$, $\lambda^{235}U = 9{\cdot}8485E - 10\ a^{-1}$, $\lambda^{238}U = 1{\cdot}55125E - 10\ a^{-1}$).

GLITTER software. Calibration was based on the NIST 612 trace element glass standard with reference values from the GeoReM database (Jochum *et al.*, 2011). ^{43}Ca was used as the internal standard for quantification of mineral analyses. Standardization was done at the beginning and the end of each analytical run to correct for instrumental drift. US Geological Survey (USGS) reference glass BCR-2G was measured as an unknown after every tenth sample spot and is in agreement with literature data.

$^{40}Ar/^{39}Ar$ incremental heating experiments were conducted on feldspar phenocryst separates at the IFM-GEOMAR Tephrochronology Laboratory (Supplementary Data 4). The minerals were hand-picked from crushed and sieved splits. All separates and chips were cleaned using an ultrasonic disintegrator. Phenocrysts were then etched in 15% hydrofluoric acid for 15 min. Samples were neutron irradiated at the 5 MW reactor of the GKSS Reactor Centre (Geesthacht, Federal Republic of Germany), with crystals chips in aluminium trays and irradiation cans wrapped in 0·7 mm cadmium foil. Samples were step-heated by laser. Purified gas samples were analyzed using a MAP 216 noble gas mass spectrometer. Raw mass spectrometer peaks were corrected for mass discrimination and background, and blank values were determined after every fifth analysis. The neutron flux was monitored using TCR sanidine (Taylor Creek Rhyolite = 27·92 Ma; Dalrymple & Duffield, 1988) and internal standard SAN6165 (0·470 Ma; Van den Bogaard, 1995). Vertical variations in J values were quantified by a cosine function fit. Lateral variations in J were not detected. Corrections for interfering neutron reactions on Ca and K are based on analyses of optical grade CaF_2 and high-purity K_2SO_4 salt crystals that were irradiated together with the samples. Ages derived from step-heating analyses are based on plateau portions of the age spectra. Plateau regions generally comprise >50% of the ^{39}Ar released and more than three consecutive heating steps that yield the same ages (within 2σ error).

Zircons were separated from a 20 kg gabbro sample using standard methods. The rocks were crushed to coarse sand size with a jaw crusher, following which zircons were concentrated by flotation, sieving, magnetic separation and heavy liquids. A representative amount of zircon with grain sizes of 50–100 μm was manually picked and mounted in epoxy resin. After polishing, cathodoluminescence (CL) images were taken using a CL detector connected to a Jeol JXA 8900 14 RL electron microprobe at the University of Mainz. U, Th and Pb isotopes were analysed by LA-ICP-MS using an Agilent 7500ce quadrupole ICP-MS system linked to a New Wave NWR193 ArF excimer laser system with 193 nm wavelength and a large format sample chamber with flexible cup that picks up the ablated material to optimize sensitivity and minimize washout times at minimum reaction times. This leads to comparable ablation conditions throughout the entire chamber including samples and standards. After pre-ablation, analyses were conducted using a 25 μm spot size with 20 s warmup time, 30 s dwell time and 30 s washout time. The repetition rate was 10 Hz at pulse energy of 7 J cm^{-2} giving a maximum sensitivity with low oxides indicated by 254/238 mass ratios below 0·5. The dwell times for single mass scans are 10 ms for masses 232 and 238, and 30 ms for 202, 204 and 208. Dwell times of 40 and 60 ms were used for masses 206 and 207 respectively. We used 0·7 l min^{-1} Ar carrier gas and 0·7 l min^{-1} He as sample gas.

For a first data reduction we used Glitter Software (Van Achterbergh *et al.*, 2000). Time-dependent laser and mass spectrometer induced inter-element fractionation (Pb/U), mass fractionation, as well as common lead, were corrected using an inhouse Excel© worksheet. The inter-element fractionation during ablation was corrected linearly. To do this, ablation conditions such as spot sizes and ablation times were kept constant during each session. When necessary, common lead was corrected using the background and Hg corrected 204 mass signals and a model Pb isotope ratio (Stacey & Kramers, 1975). The interference of ^{204}Hg was corrected by measuring ^{202}Hg and estimating the ^{204}Hg using a ratio of 0·2299. Common lead was corrected for only in zircons with significantly small 206/204 ratios so that the corrected 207/206 ratios lay outside the internal error of the uncorrected ratios (<2% rel. ^{206}Pb/^{207}Pb). Ages, errors and concordia diagrams were produced using Isoplot3-macros for Excel© (Ludwig, 2003). Concordia ages are plotted with 2σ error ellipses and discordia intercept ages are given at 95% confidence (Supplementary Data 4). Analyses were standardized using a Plesovice zircon (Slama *et al.*, 2008). The reproducibility was controlled by measuring GJ-1 and 91500 standard zircons, from Jackson *et al.* (2004) and Wiedenbeck *et al.* (1995) respectively, as blind samples; measured values deviate less than 2% from the accepted values.

RESULTS

Fresh rocks are rare in ophiolites. As alteration may have a profound effect on their chemical composition, it is necessary to understand the direction and magnitude of the various chemical changes induced by fluid–rock reaction. It is known that Li, Rb, Cs, K, U and P can show strong secondary enrichment (Hart *et al.*, 1999; Bach *et al.*, 2001). Therefore, in the subsequent presentation and discussion, we preferentially use elements and isotope ratios that are relatively insensitive to alteration, such as SiO_2, Al_2O_3, TiO_2, MgO, Fe_2O_3, HFSE, REE, Th, Ba and ^{143}Nd/^{144}Nd. Moreover, we use the major and trace element compositions of unaltered clinopyroxene grains to constrain the composition of the corresponding equilibrium melt(s) unaffected by ocean floor alteration.

Whole-rock major and trace elements

The igneous rocks of the Demir Kapija ophiolite define two geochemically distinct groups. The first group comprises gabbros, sheeted dyke diabases and pillow basalts, whereas the second includes subduction-related intrusions. The gabbros and diabases have tholeiitic characteristics, whereas subduction-related rocks are predominantly calc-alkaline (Fig. 4a).

The gabbros, sheeted dyke diabases and pillow basalts have relatively restricted SiO_2 contents with most samples ranging between 45 and 55 wt %. Rocks of this group plot in the andesite–basalt or andesite fields of the Zr/TiO_2 vs Nb/Y diagram (Fig. 4b) and in the picrite and basalt (gabbro) to trachybasalt–andesite (sheeted dyke diabases and pillow basalts) fields in the total alkalis–silica (TAS) classification scheme (Le Bas *et al.*, 1986) (Fig. 4d). They generally have lower K_2O (<1 wt %) and Al_2O_3 (12·5–15 wt %) contents and higher TiO_2 (1·5–2·7 wt %) than the subduction-related rocks (Figs 4c and 5a). The gabbros have relatively heterogeneous compositions; two samples are magnesium rich and plot in the field of primitive MORB (Fig 5a). The sheeted dyke diabases and pillow basalts have less heterogeneous compositions and are generally rich in TiO_2 (Fig. 5a). They do not show a normal MORB differentiation trend when compared with East Pacific Rise basalts, but follow a trend similar to Mariana back-arc basalts (Fig. 5a). The Ti/V ratios are high (Ti/V between 20 and 50), which is also typical of MORB and most back-arc basalts but not subduction-related basalts (Fig. 5b). Gabbros, sheeted dyke diabases and pillow basalts have subparallel incompatible trace element and REE patterns (Fig. 6a and c). Some gabbros are more depleted and have a positive Eu anomaly (Fig. 6c), owing to plagioclase accumulation. Sheeted dyke diabases and pillow basalts are less depleted in incompatible trace elements than mid-ocean ridge basalts (MORB). They are also slightly more enriched in Th and light REE (LREE) than MORB. Pronounced positive Pb

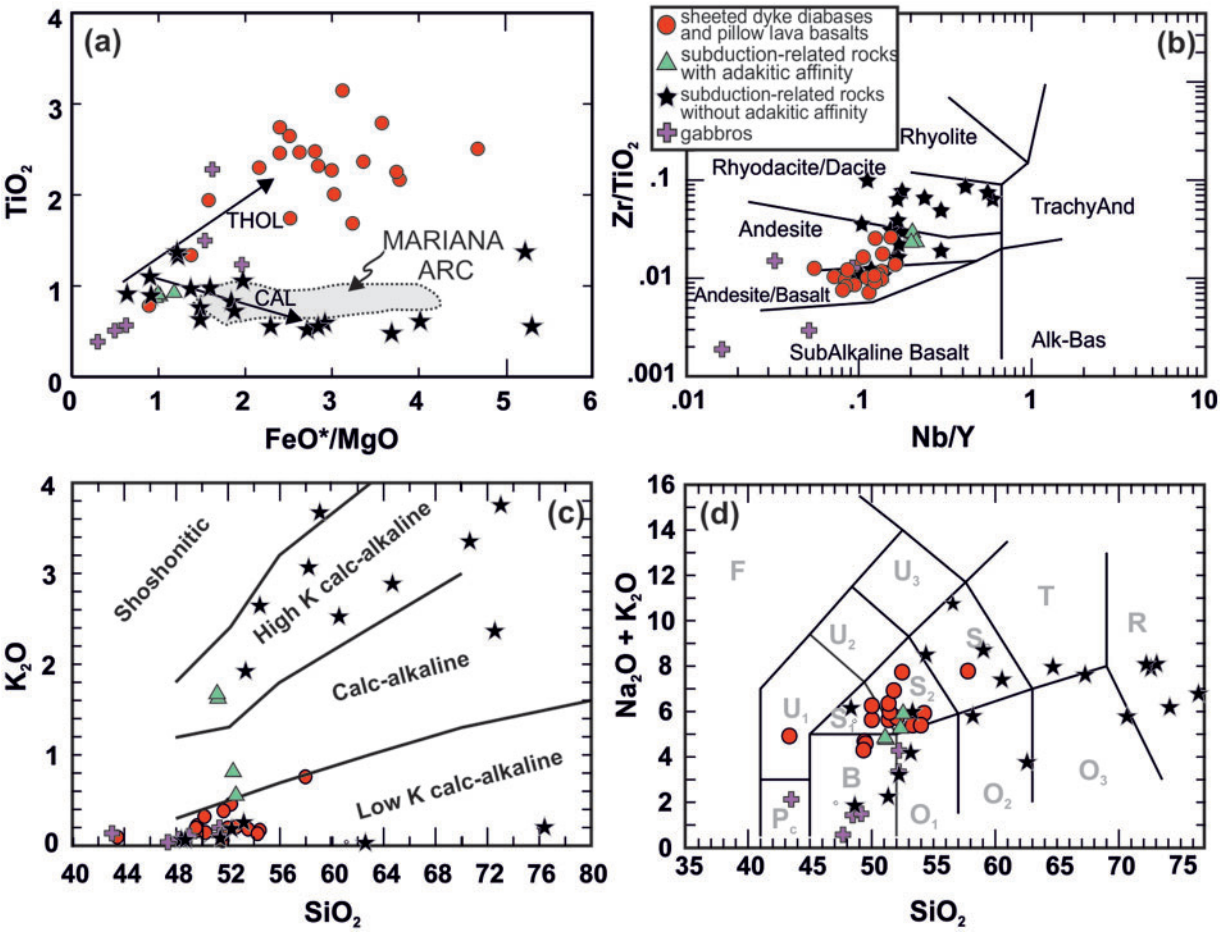

Fig. 4. Classification diagrams for the Demir Kapija igneous rocks. (a) TiO_2 wt % vs FeO*/MgO (FeO*, total iron as FeO); tholeiitic (THOL) and calc-alkaline (CAL) trends are from Miyashiro (1975). Mariana-arc data are from the GEOROC database (http://georoc.mpch-mainz.gwdg.de/georoc/). (b) and (c) Winchester & Floyd (1977) and Peccerillo & Taylor (1976) based classification diagrams. (d) $Na_2O + K_2O$ vs SiO_2 wt % (F, foidite; Pc, picrobasalt; S_1, trachybasalt; S_2, basaltic trachyandesite; S_3, trachyandesite; T, trachyte; U_1, basanite; U_2, phonotephrite; U_3, tephriphonolite; B, basalt; O_1, andesite–basalt; O_2, andesite; O_3, dacite; R, rhyolite).

and U anomalies are probably the result of hydrothermal alteration. Their REE patterns (Fig. 6c) with $(La/Yb)_n = 0{\cdot}5–2{\cdot}4$, $(La/Sm)_n = 0{\cdot}5–1{\cdot}3$ and $(Sm/Yb)_n = 0{\cdot}8–1{\cdot}2$ are relatively flat with a depletion of LREE, consistent with MORB compositions.

The subduction-related rocks plot in the basaltic andesite to dacite–rhyolite fields in the Zr/TiO_2 vs Nb/Y classification diagram of Winchester & Floyd (1977) (Fig. 4b). These rocks have a wide range of SiO_2 contents (47–73 wt %) and may be classified as basaltic-trachyandesites, trachyandesites, trachydacites and rhyolites using the TAS classification (Fig 4d; Le Bas *et al.*, 1986). Most samples have K_2O contents greater than 2·0 wt %, plotting in the high-K field in the K_2O vs SiO_2 diagram (Fig. 4c). The MgO contents in the rocks from this group range from 9 to 0·3 wt % (Fig. 5a). Ti/V is <20, similar to other arc rocks (Fig. 5b). The most distinctive feature of the subduction-related rocks is their marked depletion in Ti, Nb and Ta, and enrichment in LILE, such as U and Th, which is characteristic of volcanic rocks generated in a subduction zone environment (Fig. 6b). These rocks do not plot in the mantle field on Th/Yb and Ba/Yb vs Nb/Yb diagrams, but are shifted towards the subduction-component enriched field (Fig. 7a and b). Extreme Th enrichment and Th/Nb and Th/La exceeding unity (Fig. 7c) suggest that melts derived from subducting sediments played an important role in their petrogenesis (e.g. Patino *et al.*, 2000; Sadofsky *et al.*, 2008). Furthermore, Ba/Th vs Th and $^{143}Nd/^{144}Nd$ (Fig. 7d, inset) diagrams also indicate that the slab-derived component is dominated by sediment-derived melts, rather than by fluids. The subduction-related rocks show enriched REE patterns (Fig. 6d) with $(La/Yb)_n = 3{\cdot}56–14{\cdot}79$, $(La/Sm)_n = 2{\cdot}30–3{\cdot}70$ and $(Sm/Yb)_n = 1{\cdot}20–4{\cdot}04$. All the above features make these rocks distinct from the gabbros, sheeted dyke diabases and pillow basalts.

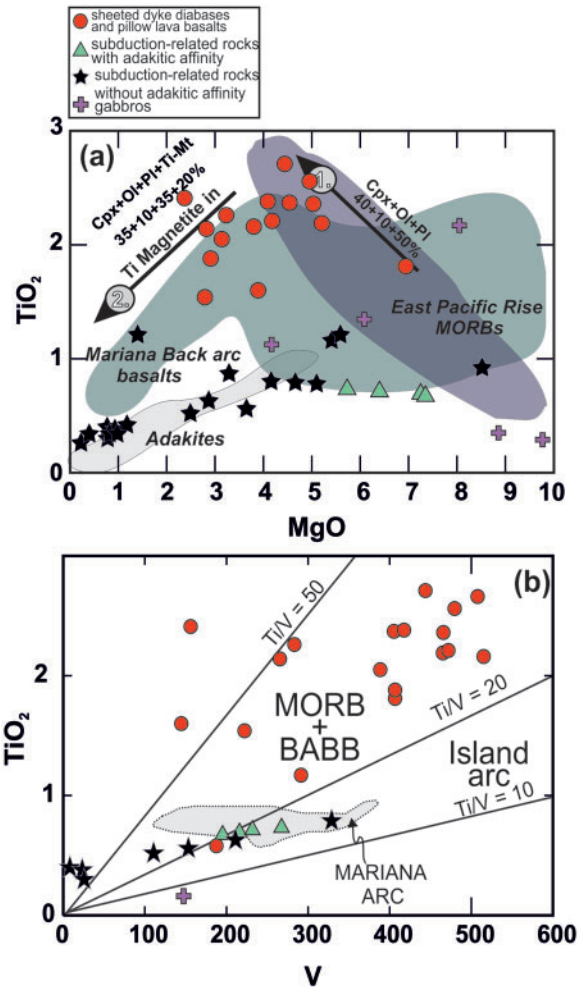

Fig. 5. (a) TiO_2 (wt %) vs MgO (wt %) for igneous rocks of the Demir Kapija ophiolite. Sheeted dyke diabases and pillow basalts show a two-step fractionation trend. Step 1 involves strong fractionation of Cpx, Ol and Pl in the proportion 40:10:50 (per cent; up to 40% fractionation), which enriched the melts in TiO_2 (up to 2·7%). High TiO_2 contents triggered crystallization of Ti-magnetite bearing assemblage in a second fractionation, step 2, which involves Cpx + Ol + Pl + Ti-Mt assemblage in the proportions 35:10:35:20. The compositions of Ol and Pl are from Deer *et al.* (1992); Mariana back-arc basalts, MORB and adakite data are from the GEOROC database (http://georoc.mpch-mainz.gwdg.de/georoc/). (b) TiO_2 (wt %) vs V (ppm). The fields for MORB + BABB and island arc basalts are from Shervais (1982) and Reagan *et al.* (2010). Mariana-arc data are from the GEOROC database (http://georoc.mpch-mainz.gwdg.de/georoc/).

Within the Demir Kapija group of subduction-related rocks we tentatively distinguish two subgroups—with and without adakitic affinity. The two subgroups are best distinguished based on their trace element characteristics, as well as Sr–Nd–Pb isotopic and clinopyroxene compositions. The REE patterns of the two Demir Kapija subduction-related subgroups show substantial differences: rocks with adakitic affinity show a higher degree of REE fractionation, with more enriched LREE and more depleted heavy REE (HREE) than the subduction-related rocks without adakitic affinity (Fig. 6d). Both subgroups show minor negative Eu anomalies. The rocks with adakitic affinity have high MgO and elevated Sr/Y and La/Yb ratios, which is typical for adakites (Defant & Drummond, 1990; Sen & Dunn, 1994; Yogodzinski & Kelemen, 1998, 2007; Martin, 1999; Calmus *et al.*, 2003; Martin *et al.*, 2005; Falloon *et al.*, 2008) (Fig. 7e and f). Adakitic affinity is the most appropriate term to describe these rocks because they have slightly lower Sr/Y and La/Yb ratios then typical adakites; only one sample plots in the adakite field(s) on standard adakite diagrams (Fig. 7e and f). Similar rocks, variably enriched in REE and Sr with adakitic affinity, have been reported from recent arcs; for example, the Aleutians, where they are termed high-Mg andesites (Yogodzinski & Kelemen, 1998, 2007). It should be noted that the rocks with adakitic affinity demonstrate mingling and mixing on an outcrop scale with rocks without adakitic affinity (Fig. 3c).

Sr, Nd and Pb isotopes

Initial Sr and Nd isotopic compositions of the volcanic rocks from the Demir Kapija ophiolite fall within a rather wide range (Fig. 8; Table 2): initial $^{87}Sr/^{86}Sr$ ranges from 0·70306 to 0·71647, and initial $^{143}Nd/^{144}Nd$ ranges from 0·51226 to 0·51276, which corresponds to εNd_T values from −3·3 to 6·5. The range of Pb isotopic compositions for the Demir Kapija rocks is even wider: 17·05–20·86 for $^{206}Pb/^{204}Pb$, 15·60–15·76 for $^{207}Pb/^{204}Pb$ and 37·28–40·45 for $^{208}Pb/^{204}Pb$ (Fig. 8).

The geochemically different (sub)groups have distinctly different Nd isotopic compositions: gabbros, sheeted dyke diabases and pillow basalts have the most radiogenic $^{143}Nd/^{144}Nd$ values; the subduction-related rocks without adakitic affinity have less radiogenic $^{143}Nd/^{144}Nd$ values; whereas those with adakitic affinity have the least radiogenic $^{143}Nd/^{144}Nd$ values (Fig. 8a). Several samples plot off the mantle array towards higher $^{87}Sr/^{86}Sr$ values, most distinctly sample 06DK16. This displacement towards more radiogenic $^{87}Sr/^{86}Sr$ may be due to the addition of seawater Sr at the emplacement level or the addition of radiogenic Sr to the source of the parent magmas by fluids derived from the dehydrating slab. Importantly, in the $^{143}Nd/^{144}Nd$ vs SiO_2 diagram (Fig. 8b), there is essentially no correlation among samples from the different groups that show similar $^{143}Nd/^{144}Nd$ values at highly variable SiO_2 contents.

The Pb isotopic compositions of the Demir Kapija rocks in part plot within the mantle array (Fig. 8c and d). The majority of rocks, however, plot slightly above the array, with more radiogenic $^{207}Pb/^{204}Pb$.

Clinopyroxene chemistry

We performed a detailed study on fresh clinopyroxene crystals retrieved from the subduction-related rocks. Representative major and trace element data are shown in

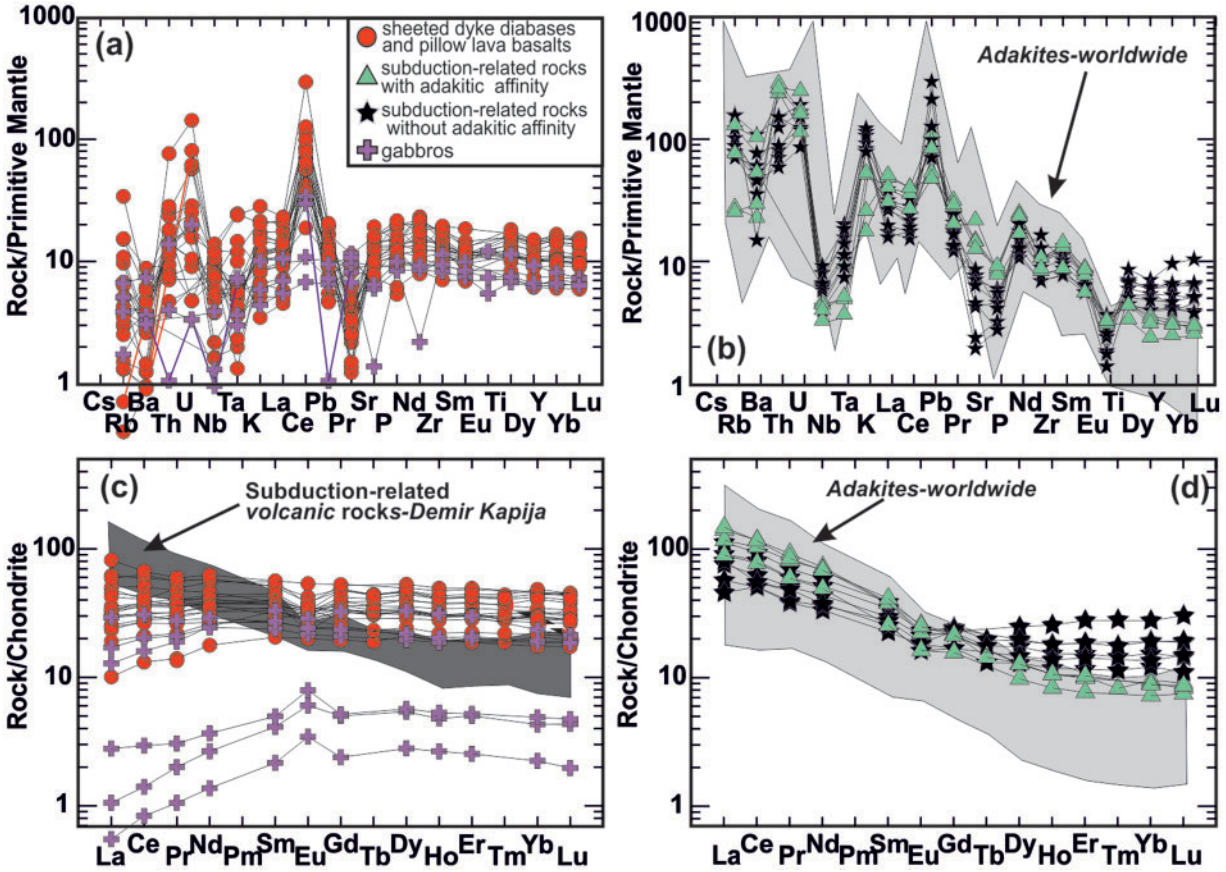

Fig. 6. Trace element characteristics of the igneous rocks of the Demir Kapija ophiolite. (a, b) Primitive mantle-normalized (Sun & McDonough, 1989) concentrations of incompatible trace elements for (a) sheeted dyke diabases, pillow basalts and gabbros, and (b) subduction-related rocks (with and without adakitic affinity). (c, d) Chondrite-normalized (Sun & McDonough, 1989) REE for (c) sheeted dyke diabases, pillow basalts and gabbros, and (d) subduction-related rocks. Adakite field from the GEOROC database (http://georoc.mpch-mainz.gwdg.de/georoc/).

Table 3. An extended discussion of their compositional variation, as well as the full dataset, is presented as Supplementary Data 5, 6 and 7.

When plotted together, clinopyroxenes from the two subgroups of subduction-related rocks define two trends that intersect at Mg-rich compositions and show a negative correlation in the Al_2O_3 vs Mg# diagram (Fig. 9a). Trend 1 is dominantly occupied by clinopyroxenes from the rocks with adakitic affinity. It is characterized by moderate variation of Al_2O_3 with small variation in Mg# at overall high Mg# (Fig. 9a). Xenocrystic clinopyroxenes from rocks without adakitic affinity plot within this trend, although in part at slightly lower Mg#. Trend 2 (Fig. 9a) is characterized by a gentler slope in the Al_2O_3 vs Mg# diagram and is typical for clinopyroxenes from rocks without adakitic affinity. The low-Al_2O_3 segment of the slope overlaps at high Mg# compositions with Trend 1, whereas the high-Al_2O_3 segment comprises the highly evolved compositions of clinopyroxenes from the rocks without adakitic affinity (Fig. 9a). The resorbed 'green cores' (Fig. b in Supplementary Data 4) and green zones (Fig. c in Supplementary Data 4) of clinopyroxenes from the rocks with adakitic affinity also plot within Trend 2 (Fig. 9).

The trace element compositions demonstrate substantial differences between the clinopyroxenes from different subgroups (Fig. 9c and d). High-Mg# clinopyroxenes from the rocks with adakitic affinity show a high degree of LREE enrichment and HREE depletion (La/Yb >2; Dy/Yb mostly >1·5 and up to seven), as well as a high Sr/Y ratio (up to 11·5). Relative to them, the majority of clinopyroxene crystals from the rocks without adakitic affinity have lower Sr abundances, giving rise to lower Sr/Y ratios (Fig. 9c). Their REE distribution patterns are flatter (Fig. 9d), resulting in systematically lower La/Yb and Dy/Yb ratios (Fig. 9c and d). Furthermore, they show stronger Eu anomalies. Importantly, low-Mg xenocrystic 'green cores' and zones in the grains from the rock with adakitic affinity have similarly flat REE patterns and strong Eu anomalies, as well as low Sr/Y and high Sc contents (Fig. 9b–d), demonstrating that they ultimately

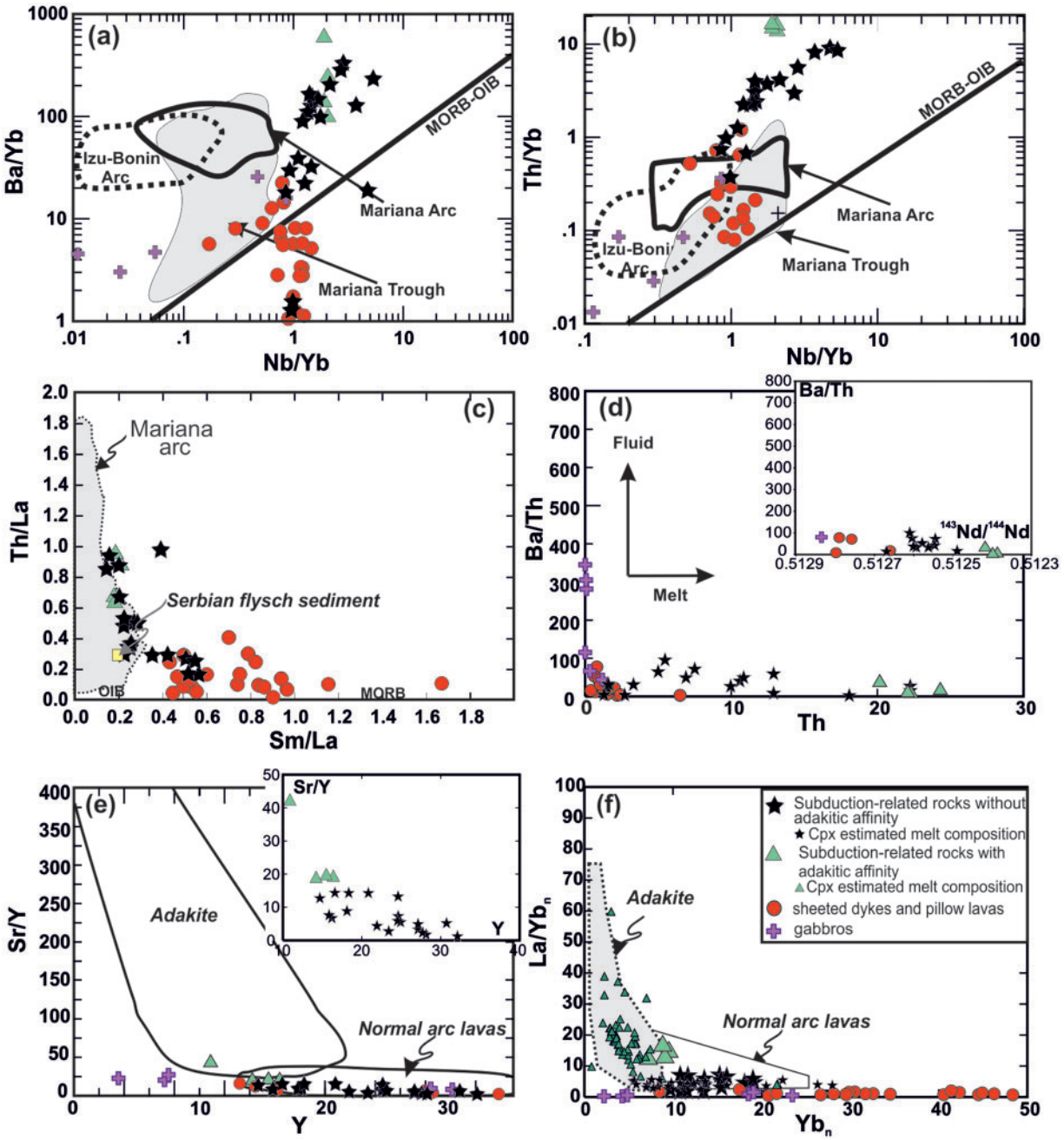

Fig. 7. Trace element ratio–ratio plots for igneous rocks of the Demir Kapija ophiolite. (a) Nb/Yb vs Ba/Yb and (b) Nb/Yb vs Th/Yb (Pearce & Peate, 1995). Data for the Izu–Bonin Arc, Mariana Arc and Mariana Trough are from Ishizuka *et al.* (2010). OIB, ocean-island basalt. (c) Sm/La vs Th/La. Data for Mariana Arc and Serbian flysch sediments from Ishizuka *et al.* (2010) and Prelević *et al.* (2008). (d) Th vs Ba/Th and Ba/Th vs $^{143}Nd/^{144}Nd$ (inset). (e) Y vs Sr/Y, discriminating normal arc lavas from adakites. Adakite field after Defant & Drummond (1990). Inset: enlarged view of the same dataset. (f) Yb_n vs La/Yb_n (n denotes chondrite normalization). The partition coefficients used for calculation of the composition of the melts in equilibrium with Demir Kapija Cpx (Cpx-estimated melt composition) are taken from Sobolev *et al.* (1996). Adakite field after Defant & Drummond (1990).

originated from a magma without adakitic affinity. These grains are mantled by clinopyroxene of a composition that is typical for rocks of adakitic affinity (see Fig. 9b and d, where these two contrasting REE patterns occur in one single grain). Complex compositional variations observed in the clinopyroxenes from both subgroups closely resemble the composition of adakitic and non-adakitic clinopyroxene from Aleutian arc volcanic rocks (Fig. 9c). The presence of xenocrystic clinopyroxenes in both subgroups of subduction-related lavas indicates open-system

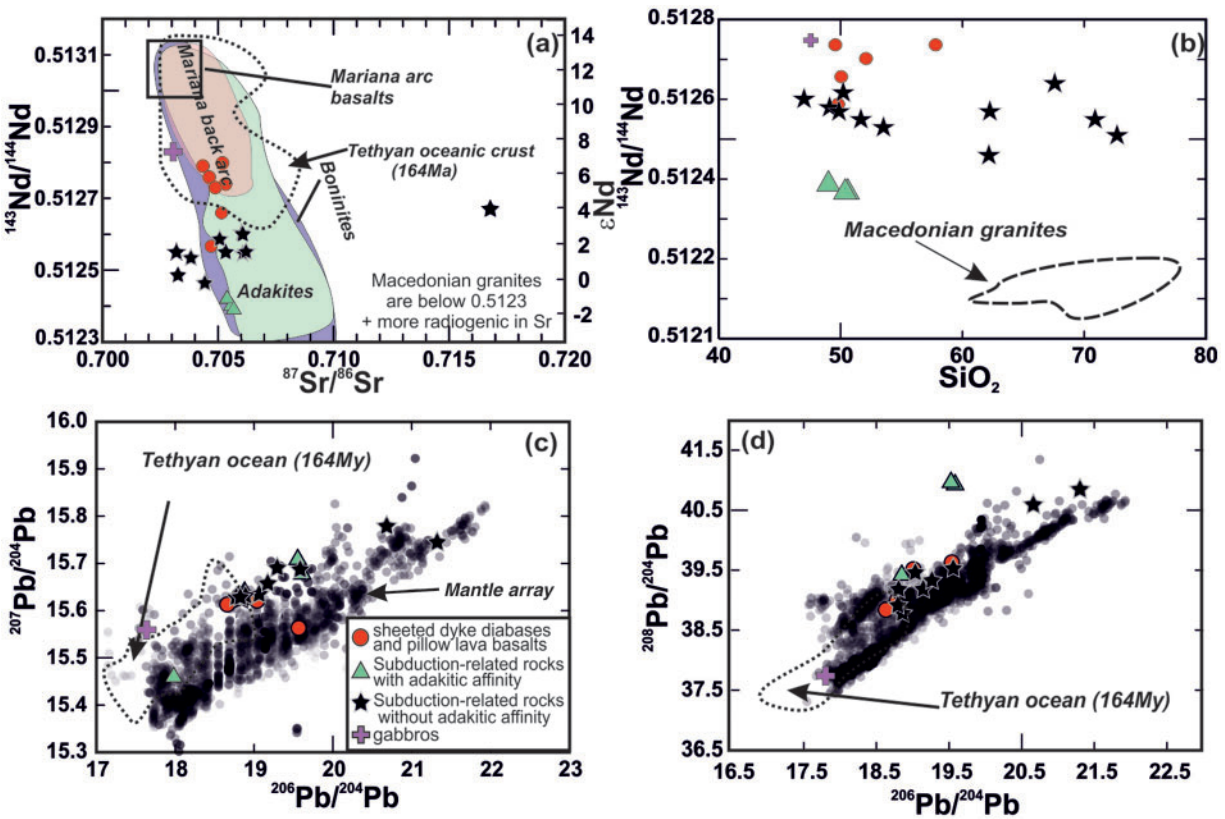

Fig. 8. Sr–Nd–Pb isotopic variations in the igneous rocks of the Demir Kapija ophiolite. (a) $^{87}Sr/^{86}Sr$ vs $^{143}Nd/^{144}Nd$. Reference field for Tethyan Ocean is from Zhang *et al.* (2005). Data for Mariana arc basalts, Mariana back-arc basalts, boninites, adakites and the mantle array are from Reagan *et al.* (2010) and http://georoc.mpch-mainz.gwdg.de/georoc/. Macedonian granites from Šarić *et al.* (2009). (b) SiO_2 vs $^{143}Nd/^{144}Nd$. Macedonian granite field from Šarić *et al.* (2009). (c) $^{206}Pb/^{204}Pb$ vs $^{207}Pb/^{204}Pb$. (d) $^{206}Pb/^{204}Pb$ vs $^{208}Pb/^{204}Pb$. Mantle array is from http://georoc.mpch-mainz.gwdg.de/georoc.

processes such as magma mixing or mingling between these two melt types, as already recognized on an outcrop scale (Fig. 3c).

Age constraints

The age of the altered and metamorphosed volcanic rocks from the Demir Kapija ophiolite has so far only been poorly constrained by published K/Ar ages for the Demir Kapija diorite (145–154 Ma) and gabbro (149–165 Ma; Spray *et al.*, 1984; Boev & Lepitkova, 2002). Palaeontological data are available from carbonate formations that—together with terrigeneous layers and basal breccia–conglomerates—demonstrate a transgressive relationship with the Demir Kapija ophiolite block. The micro-fauna places these limestones within the Upper Jurassic (Tithonian; Boev & Lepitkova, 2002), which may be considered as a minimum age for the ophiolite.

In the course of this study representative samples from each group were selected for dating. Zircon was obtained only from one gabbro sample and gave an age of 166·4 ± 1·2 Ma (Supplementary Data 4), which coincides with the U–Pb zircon crystallization age of 166 ± 1·8 Ma reported for the Guevgelia gabbro (Zachariadis, 2007). This gabbro age is slightly older than the age of the subduction-related rocks. Feldspar from one sample of the subduction-related rocks gave an Ar–Ar age of 164 ± 0·5 Ma (Supplementary Data 4), which is in agreement with published Ar–Ar and U–Pb data for felsic volcanic rocks from the Greek part of the ophiolite (Christofides *et al.*, 1990; Anders *et al.*, 2005; Zachariadis, 2007). Thus, isotopic age determinations demonstrate that the emplacement of the ophiolite gabbro and the formation of the subduction-related rocks in Demir Kapija was very close in time.

DISCUSSION

The magmatic rocks of the Demir Kapija ophiolite comprise two magmatic suites: (1) gabbros, sheeted dyke diabases and pillow basalts representing former oceanic crust, which was intruded shortly after its genesis (by not more than a few million years) by (2) subduction-related volcanic rocks with and without adakitic affinity.

Table 3: Representative analyses of clinopyroxene types occurring in subduction-related lavas from the Demir Kapija ophiolite

	Cpx from lavas with adakitic affinity				Cpx from lavas without adakitic affinity		
	Homogeneous high Mg		Green cores				
wt %							
SiO_2	53·0	52·7	49·9	50·0	52·7	51·4	52·2
CaO	21·2	21·9	20·7	20·5	21·3	20·8	20·6
TiO_2	0·3	0·3	0·6	0·6	0·3	0·8	0·7
FeO	6·0	5·5	9·0	8·8	5·6	9·6	9·3
Al_2O_3	1·9	2·1	3·1	3·0	2·1	3·7	3·3
MgO	18·3	17·8	15·4	15·4	17·3	13·8	14·4
Na_2O	0·2	0·1	0·3	0·3	0·1	0·2	0·3
Cr_2O_3	0·1	0·1	0·0	0·0	0·0	0·0	0·0
MnO	0·2	0·1	0·3	0·3	0·2	0·3	0·3
Sum	100·9	100·6	99·3	98·8	99·7	100·6	101·0
Mg#	84·5	85·2	75·3	75·7	84·5	72·0	73·3
ppm							
Li	1·97	0·72	1·099	0·9		<3·62	<3·32
Sc	84·3	87·2	243	235		195	193
V	212	213	242	264		523	585
Cr	245	281	<1·43	<1·06		<9·31	<7·43
Co	50·6	44·7	30·6	31·4		48·8	52·3
Ni	188	180	1·00	1·00		6·25	5·02
Rb	0·321	<0·21	<0·125	0·355		<0·601	<0·532
Sr	41·9	47·2	36·8	34·7		26·4	24·2
Y	9·66	8·94	50·4	50·5		30·2	34·1
Zr	12·0	12·0	32·4	31·6		33·3	34·9
Nb	<0·145	<0·074	<0·041	<0·037		<0·342	<0·251
Cs	<0·137	<0·112	<0·071	<0·057		<0·263	<0·242
Ba	<0·802	0·791	0·256	0·692		2·07	<1·53
La	2·03	2·04	2·89	2·66		1·96	1·86
Ce	7·66	8·61	14·4	14·9		8·66	7·54
Pr	1·48	1·61	3·05	2·95		1·88	1·51
Nd	8·31	9·43	20·9	19·5		10·0	13·1
Sm	3·31	2·37	8·53	8·38		3·57	3·63
Eu	0·680	0·722	2·18	2·24		1·40	1·41
Gd	2·09	2·08	10·7	10·2		5·95	5·54
Tb	0·288	0·358	1·63	1·39		0·790	1·11
Dy	2·39	2·26	10·7	10·9		6·04	4·91
Ho	0·444	0·390	2·17	2·38		1·05	1·14
Er	0·780	0·910	6·10	5·96		3·22	3·57
Yb	0·610	0·660	4·66	4·65		2·93	4·08
Lu	0·267	0·156	0·649	0·662		0·720	0·490
Hf	0·500	0·495	1·61	1·63		1·91	2·45
Ta	<0·089	<0·038	<0·029	<0·020		<0·185	<0·171
Th	0·126	0·084	0·052	0·068		0·171	<0·168
U	<0·073	<0·019	0·235	<0·016		<0·137	<0·103
Dy/Yb	3·92	3·42	2·30	2·36		2·06	1·20
Sr/Y	4·33	5·28	0·73	0·69		0·87	0·71
En	0·56	0·55	0·51	0·53	0·54	0·49	0·50
Wo	0·41	0·42	0·44	0·42	0·42	0·45	0·45
CaTsch	0·03	0·04	0·05	0·05	0·04	0·07	0·06

Extended presentation and the full dataset are presented as Supplementary Data 5, 6 and 7.

Demir Kapija sheeted dykes and pillow basalts: back-arc basin basaltic ocean crust

The large range of SiO_2 and MgO contents, along with the systematic variations of TiO_2, Al_2O_3 and Fe_2O_3 vs MgO, implies that fractional crystallization controls the geochemistry of the sheeted dyke diabases and pillow basalts. The low abundance of compatible trace elements also indicates that these rocks are well evolved.

Major element variation in MORB is a function of the continuous evolution of the parental basaltic melts along the Ol + Pl and Ol + Pl + Cpx cotectics (Almeev *et al.*, 2008, and references therein). The liquid line of descent shows an increase in Fe_2O_3 and a decrease of Al_2O_3 with falling MgO, owing to Ol + Cpx + Pl fractionation (Grove *et al.*, 1992). The sheeted dyke diabases from Demir Kapija, however, define a much broader compositional range than typical MORB and show a higher extent of differentiation, as reflected in the predominance of samples with <5% MgO (Fig. 5a). The differentiation trends show the simultaneous increase of SiO_2 and Al_2O_3 and a decrease of FeO and TiO_2 with decreasing MgO (Fig. 5a). Modelling indicates a fractionating assemblage that is unusual for MORB magmas as a considerable amount of Ti-magnetite seems to be involved (Fig. 5a). The high TiO_2 contents of the Demir Kapija ophiolite mafic sequence shown in Fig. 5a can be reproduced if the primary melts experienced up to 40% of fractionation of Ol + Cpx + Pl, which increased the TiO_2 content to ~2·5% at about 5% MgO. Later fractionation of the same assemblage + Ti-magnetite can explain the major element trends for the diabases and pillow basalts of the Demir Kapija ophiolite. Some experiments have demonstrated high saturation levels of TiO_2 in basaltic melts (Green & Pearson, 1986;

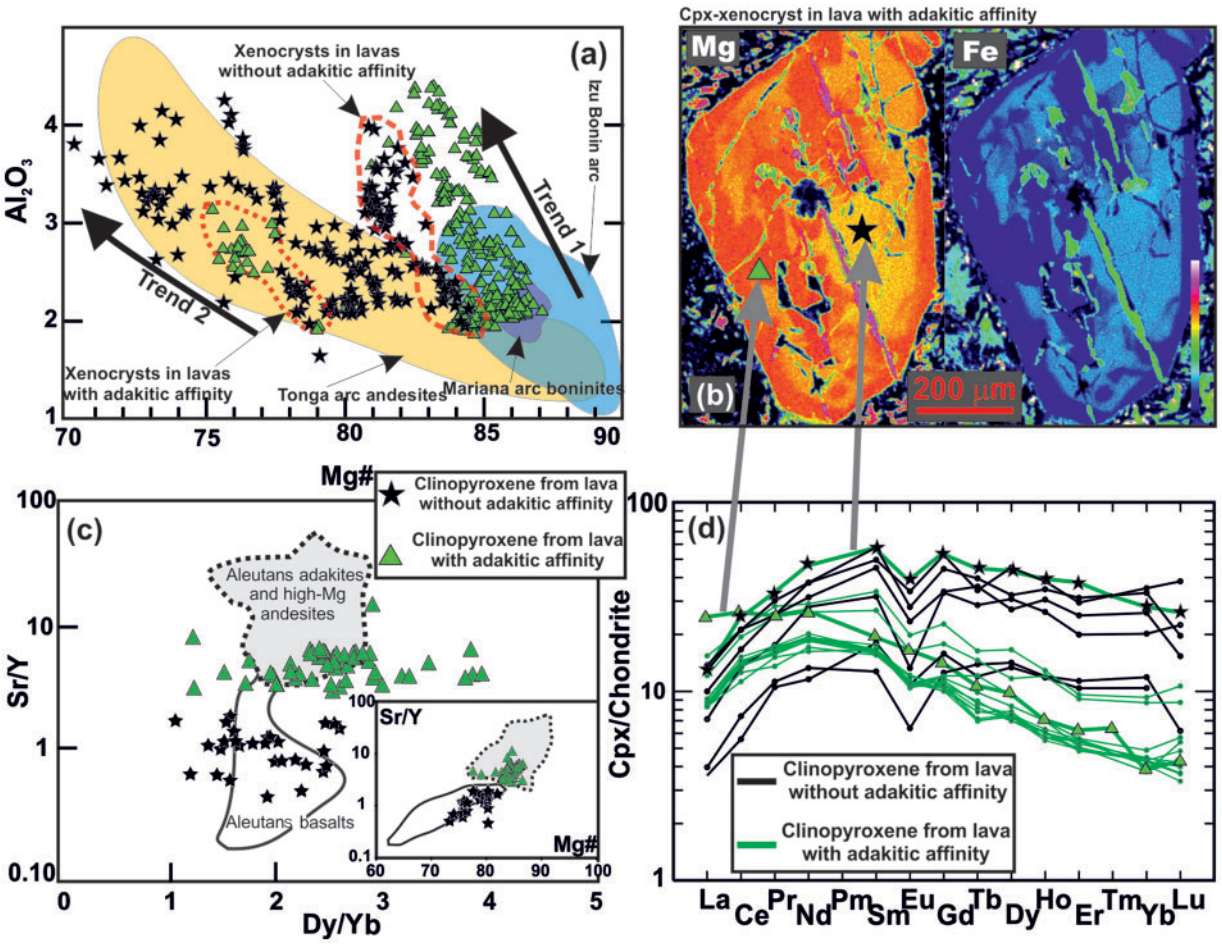

Fig. 9. Major and trace element variation diagrams for clinopyroxene from the Demir Kapija subduction-related volcanic rocks. (a) Mg# vs Al_2O_3. Clinopyroxene data for Mariana arc boninites, Tonga arc andesites and Izu–Bonin arc (andesites and boninites) are from the GEOROC database (http://georoc.mpch-mainz.gwdg.de/georoc/). (For explanation of Trends 1 and 2 see the main text.) (b) Element-distribution maps (Mg and Fe) of a clinopyroxene from the lava with adakitic affinity. The grain is a heavily resorbed xenocryst from a lava with adakitic affinity, which originated from a lava without adakitic affinity. (c) Dy/Y and Mg# (inset) vs Sr/Y in clinopyroxene from the Demir Kapija subuction-related volcanic rocks. Clinopyroxene from Aleutian adakites, high-Mg andesites and basalts from Yogodzinski & Kelemen (1998, 2007). (d) Chondrite-normalized (Sun & McDonough, 1989) REE patterns of clinopyroxenes from subduction-related lavas. Bold lines and symbols denote the analyses from specific locations in the grain in (b). These substantially different REE compositions found in a single grain illustrate its xenocrystic nature.

Ryerson & Watson, 1987) indicating that at 1000°C the saturation level of TiO_2 is around 2·0 wt % at pressures of 20–30 kbar. The reported TiO_2 concentration of modern MORB varies from 0·73 to 2·09 wt % in Atlantic MORB and 0·89–1·89 wt % for Central Indian ridge basalts. On the other hand, the comparably evolved compositions with variable TiO_2 concentrations observed in the Demir Kapija mafic rocks are found in back-arc basin basalts (BABB) of the western Pacific (e.g. of the Mariana back-arc; Fig. 5). The back-arc origin of the Demir Kapija sheeted dyke diabases and pillow basalts is further supported by their trace element and isotopic compositions. These rocks have pronounced negative HFSE anomalies and flat REE patterns, reflecting contamination of their mantle source with subduction-related fluids and/or melts (Pearce & Stern, 2006, and references therein). This contamination is also seen in their Nd isotopic composition, which is slightly less radiogenic than that of typical MORB (Fig. 8).

The high Ti/V and Yb/V ratios of the Demir Kapija sheeted dyke diabases and pillow basalts (Fig. 5b), similar to those of basalts from mid-ocean ridges and back-arc basins, rule out a fore-arc origin. Ti/V and Yb/V in MORB and most back-arc basin lavas are higher than in subduction-related basalts owing to a more oxidizing environment and higher V incompatibility in the latter (Shervais, 1982). Moreover, these element ratios, which are used to discriminate between fore-arc tholeiites and basalts from mid-ocean ridges and back-arcs, seem to indicate a previous depletion of the mantle source (Shervais, 1982; Reagan *et al.*, 2010).

Arc intrusions: coeval lavas with and without adakitic affinity

Intermingling features within the arc intrusions (Fig. 3c) imply that magmas with and without adakitic affinity are coeval and are related to simultaneous source processes. The Mg# >60 of the most primitive subduction-related rocks and the presence of high-Mg clinopyroxene indicate that their parental magmas are generated within the mantle (Beard & Lofgren, 1991; Rapp *et al.*, 1991).

Constraining the composition of the primary melts

On most Harker variation diagrams, both subduction-related subgroups plot along trends that could represent either differentiation or mixing (Fig. 5). However, the less radiogenic $^{143}Nd/^{144}Nd$ of the rocks with adakitic affinity (Fig. 8a) and considerably steeper REE patterns (Fig. 6d) preclude these magmas representing parental magmas for the rocks without adakitic affinity, and vice versa (Fig. 8b).

This interpretation is further supported by the major and trace element characteristics of clinopyroxenes within the two subduction-related subgroups (Fig. 9a–d). The clinopyroxene compositions systematically vary in terms of Mg#, Al_2O_3 and TiO_2, defining two clearly different compositional arrays (Fig. 9a). The major element composition, in particular the wollastonite and Ca-Tschermak components, may significantly influence the partitioning of trace elements in clinopyroxene (Gaetani & Grove, 1995). In clinopyroxenes from both subduction-related subgroups, however, the wollastonite component is relatively constant and the Ca-Tschermak component is less than 0·25 (Table 3). This suggests that the trace element partitioning in clinopyroxenes from the two subgroups is broadly similar and is not influenced by their major element compositions. Therefore, the trace element composition of the clinopyroxenes and published partition coefficients can be used to infer the composition of the equilibrium melts. The strong contrast in the trace element content of these clinopyroxene phenocryts, illustrated by the different extent of LREE/HREE fractionation (Fig. 9c and d), strictly reflects the contrasting trace element composition of their respective parental melts. This is particularly applicable when using element ratios such as LREE/HREE and middle REE (MREE)/HREE as shown below. Different trace element patterns (Fig. 9d) cannot be compromised by a fractionation relationship from fundamentally similar parental melts; thus the involvement of different parental melts is indicated. Such compositional variation is also indicated in clinopyroxene phenocrysts from Aleutian high-Mg andesites and basalts (Yogodzinski & Kelemen, 1998, 2007). The clinopyroxene phenocrysts from the rocks with adakitic affinity carry an 'adakitic' signature (elevated Sr, Sr/Y and Dy/Yb), indicating their crystallization from a 'proto-adakitic' melt that has a stronger adakitic signature than the lavas (Fig. 7f). On the other hand, the clinopyroxenes from lavas without an adakitic affinity must be derived from a different parental melt, similar in composition to common arc magmas (Fig. 7f).

The lavas from the two subduction-related subgroups (proto-adakitic and common arc melts) have high Th/Yb, Th/La and low Ba/Th, supporting the interpretation that the mantle source of the magmas was modified by sediment-derived melts rather than by fluids (Rogers *et al.*, 1985; Hawkesworth *et al.*, 1997; Plank, 2005). Plots of Ba/Th vs Th and $^{143}Nd/^{144}Nd$ (Fig. 7d and inset) are particularly effective in discriminating igneous members of the Demir Kapija ophiolite in terms of involvement of a sedimentary component. Both subduction-related subgroups record sedimentary input; the highest amount of the sedimentary component is seen in rocks with adakitic affinity. Figure 10 shows the variation of Dy/Yb, La/Yb and Sr/Y versus whole-rock $^{143}Nd/^{144}Nd$ of the lavas as well as of the melts inferred to be in equilibrium with the two subgroups of clinopyroxene based upon the measured trace element concentrations in clinopyroxene and the partition coefficients of Sobolev *et al.* (1996). $^{143}Nd/^{144}Nd$ is used as a proxy for sediment-derived melt input. Anti-correlation of Dy/Yb, La/Yb and Sr/Y with $^{143}Nd/^{144}Nd$ (Fig. 10) suggests that the adakitic signal increases with a higher input of sediment-derived material. The adakitic signature reflects the characteristics of the sediments, the melts derived from the sediments and the residual phases. The behaviour of HREE, Y and Sr is controlled by the presence of residual garnet. The rocks with adakitic affinity show the strongest adakitic signature coupled with the highest contribution of the sediment-derived melt, whereas the rocks without adakitic affinity show a lesser involvement of sediment-derived melt (Fig. 10).

The amount of sediment input can be estimated using trace element ratios and assuming that variations in the $^{143}Nd/^{144}Nd$ of subduction-related lavas are dominantly controlled by the melting of the subducted slab (Fig. 10). The bulk slab composition is modelled as a mixture of terrigeneous sediments from the Vardar Zone (Prelević *et al.*, 2008) and the oceanic crust composition represented by the Demir Kapija gabbros. This modelling shows that up to 15% sediment contribution is present in magmas without adakitic affinity, as opposed to up to 20% in magmas with adakitic affinity. Details of the composition of the slab components are given in the caption of Fig. 10.

In summary, our data suggest that melts derived from the crustal part of the subducted slab play an important role in the origin of the magmas. Given the low SiO_2 and high MgO contents of the most primitive lavas, with and without adakitic affinity (Rapp *et al.*, 1991, 1999), it is likely that slab-derived melts first reacted with the mantle wedge (Rapp *et al.*, 1999). Interaction with mantle peridotite would raise the Mg# and Cr and Ni content of

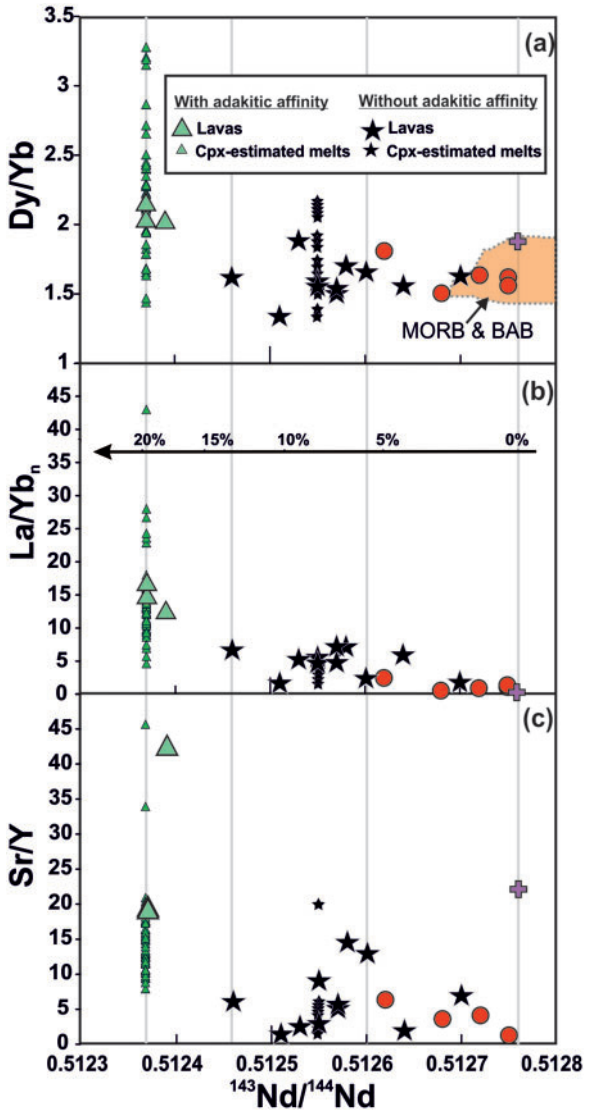

Fig. 10. $^{143}Nd/^{144}Nd$ vs (a) Dy/Yb, (b) La/Yb_n (chondrite normalized) and (c) Sr/Y for igneous rocks of the Demir Kapija ophiolite. The trace element ratios in the melts in equilibrium with both clinopyroxene subgroups from the subduction-related lavas are shown for comparison. The partition coefficients used for calculation of the composition of the equilibrium melts are from Sobolev *et al.* (1996). The horizontal arrow in (b) indicates the amount of sedimentary input in the source of the Demir Kapija subduction-related lavas. The sedimentary component is modelled as a mixture of terrigeneous sediment from the Vardar Zone with $^{143}Nd/^{144}Nd = 0{\cdot}51200$ and Nd = 26 ppm (Prelević *et al.*, 2008) and the oceanic crust composition is represented by the Demir Kapija gabbros with $^{143}Nd/^{144}Nd = 0{\cdot}512760$ and Nd = 6 ppm (see text for details).

slab-derived melts without significantly changing their trace element ratios (such as Th/La, Sr/Y, Dy/Yb; e.g. Rapp *et al.*, 1999). Substantial differences in terms of isotopic and trace element signatures in the two primary melts, recorded also in their clinopyroxene compositions, provide strong arguments against high-pressure fractionation of garnet from a 'common' arc magma in generating the Demir Kapija arc magmas with a 'slab melting' signature (Castillo *et al.*, 1999; Macpherson *et al.*, 2006).

Attempts to constrain the residual mineralogy of the source of the subduction-related lavas

Figure 11 shows modal batch-melting modelling of the variation of La/Yb vs Dy/Yb, using different source mixtures of the slab component represented by local oceanic crust and a sediment component from the Vardar Zone (Prelević *et al.*, 2008). Our aim was to explore whether different proportions of the sediment component input or source mineralogy are responsible for the trace element signature of the subduction-related lavas and their clinopyroxene phenocrysts. The variation of these ratios provides constraints on the residual source mineralogy during the prograde metamorphic path (see caption to Fig. 11 for the modal mineralogy of the source and the mineral proportions). Calculated melt trajectories demonstrate that magmas without adakitic affinity may be produced by extensive partial melting of a slab–sediment mixture with residual amphibole. Involvement of small amounts of the sediment component (less than 10%; not shown) results in lower La/Yb ratios, such as those found in the most depleted samples. It should be noted that the Dy/Yb ratio is not sensitive to the amount of sediment component involved. This ratio increases only when garnet appears as a residual mineral. Calculated melt trajectories with residual garnet + amphibole provide a reasonable fit to the data for the rocks with adakitic affinity. The melts inferred to be in equilibrium with clinopyroxene show more pronounced compositional variation and define steeper slopes than the host-rocks from which they originated (Fig. 11). The melts in equilibrium with clinopyroxene from rocks with adakitic affinity have high La/Yb and Dy/Yb ratios, which implies a source with residual garnet, but without amphibole (Fig. 11). The variation of the key trace element ratios within single clinopyroxene phenocrysts (Fig. 11) suggests mixing between different melt batches derived from different subduction-related primary melts.

If the modelled residual assemblages are interpreted in terms of different prograde metamorphic transformations of the mixture between subducted oceanic crust and sediment, it could be concluded that progressive melting of the slab + sediment has taken place at different metamorphic grades, starting at amphibolite facies and continuing to garnet amphibolite and finally to eclogite facies. However, a prograde pressure change of 10–18 kbars cannot take place in the short time span required by the coeval occurrence of the two subduction-related subgroup lavas. Therefore, we conclude that slab melting must have taken place in a narrower pressure range over an anomalously hot mantle wedge, resulting in the melting out of amphibole. Metasedimentary rocks partially melt via reactions consuming biotite at temperatures in excess of 800°C and pressures

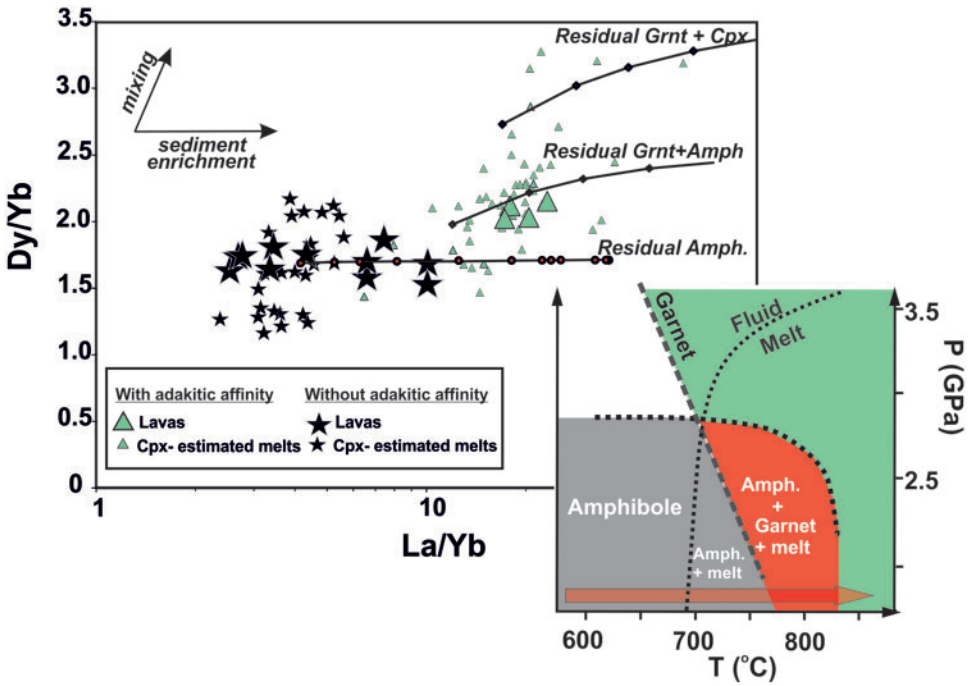

Fig. 11. La/Yb vs Dy/Yb for subduction-related lavas from the Demir Kapija ophiolite and melts in equilibrium with both clinopyroxene subgroups. The lavas without adakitic affinity follow the flat melting curve (bulk modal melting model) of a mixture between 10% terrigeneous sediment from the Vardar Zone (Prelević *et al.*, 2008) and 90% oceanic crust with a composition represented by the Demir Kapija gabbros with amphibolite-facies mineralogy (60% amphibole, 40% plagioclase). The lavas with adakitic affinity, and the melts estimated from their clinopyroxenes, follow the melting path of a different source composition and residual mineralogy (see text for details). This source is modelled as a mixture of 25% terrigeneous sediment from the Vardar Zone (Prelević *et al.*, 2008) and 75% oceanic crust represented by the Demir Kapija gabbros with garnet-amphibolite (35% amphibole, 60% plagioclase, 5% garnet) and eclogite-facies mineralogy (20% clinopyroxene, 20% garnet and 60% quartz). Mineral–melt distribution coefficients (K_d) used in the calculations: clinopyroxene from Sobolev *et al.* (1996); amphibole from Tiepolo *et al.* (2007); garnet from Johnson (1998). Inset: simplified P–T stability limits of amphibole and garnet in subducted sediments, modified from Hermann & Spandler (2008). The horizontal arrow denotes the proposed melting path for the Demir Kapija subducted crust.

of 10–20 kbar (Johnson & Plank, 1999), whereas meta-gabbroic rocks and other K-poor plagioclase-bearing igneous rocks melt predominantly via reactions consuming amphibole and plagioclase at similar temperatures and pressures. For both rock types, the stability of amphibole and garnet will critically influence the trace element behaviour. The inset in Fig. 11 shows simplified P–T stability fields for these two minerals in subducted sediments (after Hermann & Spandler, 2008), and a schematic melting path. During progressive melting (≥20%) at pressures <30 kbar, the residual assemblage will change from amphibole bearing to dominantly garnet bearing, without pressure change. Accordingly, during partial melting of a garnet-amphibolite source, amphibole will progressively melt out leaving an eclogite-like residual mineralogy. This kind of progressive melting scenario has been proposed for some eclogite-like occurrences in Archaean terranes, such as the Lewisian Complex, NW Scotland (Johnson *et al.*, 2012), where high-degree melting of mafic assemblages originally containing amphibole and plagioclase led to the formation of an eclogite-like residual mineral assemblage, owing to hotter geotherms in the late Archaean.

The above scenario provides an explanation for the occurrence of Demir Kapija subduction-related lavas with contrasting affinities. The required coincidence of partial melting of amphibolite and garnet-amphibolite sources may have been reached without significant pressure change by rising temperatures within the subducted slab at <30 kbar. This kind of thermal scenario, however, is achieved only in unusually hot arcs such as during subduction initiation of young oceanic lithosphere (Stern & Bloomer, 1992; Peacock *et al.*, 1994).

The origin of the silica-rich subduction-related lavas

Felsic lavas with SiO_2 >65%, such as those from Demir Kapija, are unusual but occur in a number of active oceanic arcs. Our modelling (Fig. 12) suggests that fractional crystallization of a parental magma without adakitic affinity cannot account for the range of silica-rich compositions of up to 74% by fractionating Mt, Ol, Pl and Cpx in different proportions (see caption of Fig. 12 for the mineral proportions used in the modelling). Instead, mixing with a high-silica anatectic melt is necessary to generate high-silica melts without adakitic affinity. This anatectic melt

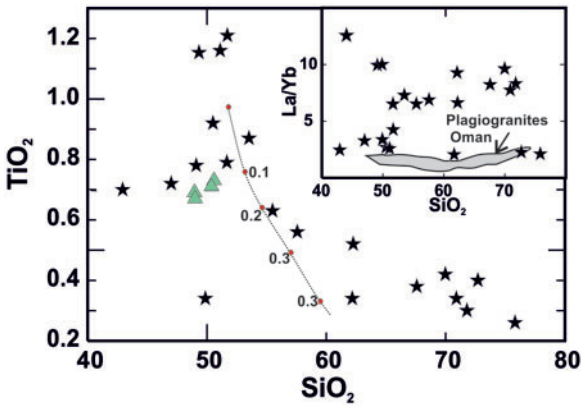

Fig. 12. Variation of TiO_2 vs SiO_2 (wt %) to evaluate the role of fractionation in the origin of high-silica subduction-related lavas. Modelled trajectory represents the fractionation of the assemblage 20% Mt + 20% Ol + 60% Pl. Inset: SiO_2 vs La/Yb in the subduction-related lavas without adakitic affinity, indicating the LREE-enriched composition of the high-silica end-member. Oman plagiogranites from Rollinson (2009). Symbols as in previous figures.

can also account for the enrichment in LILE and LREE (Fig. 12 inset). The trace element enrichment rules out the involvement of anatectic melts derived from typical oceanic plagiogranites (Pearce *et al.*, 1984; Koepke *et al.*, 2004, 2007; Rollinson, 2009). Compositional data indicate that the silica-rich melt was titanium and alumina poor and had a low Mg# and high K_2O content. It may have the following major element composition (in wt %): $SiO_2 > 74$, $Al_2O_3 < 13{\cdot}5$, $Fe_2O_3 < 1$, $MnO < 0{\cdot}5$, $MgO < 0{\cdot}5$, $CaO < 0{\cdot}8$, $Na_2O \sim 2$, K_2O 4–5, $P_2O_5 \sim 0{\cdot}05$; and Mg# 30–40. Furthermore, it should have radiogenic $^{143}Nd/^{144}Nd$, similar to the diabases (Fig. 8a). A melt of such a composition could result from the melting of immature arc crust during the early stages of arc development. Anatexis of the oceanic crust, which is hydrothermally altered and may resemble MORB gabbros and/or mafic subduction-related rocks, is possible in the early stage of arc development (e.g. 0.5–1.0 Myr after subduction initiation), within the fertile arc crust (Smith *et al.*, 2003).

From the ridge to the island arc: magma genesis during subduction initiation

Studies of subduction-related volcanism indicate that slab-derived magmas may represent an important component in the source of adakites and high-Mg andesites. Experimental data and numerical modelling (Peacock, 1990; Peacock *et al.*, 1994; Rapp & Watson; 1995; Rapp *et al.*, 1999, 2008) demonstrate that partial melting of subducted basaltic crust and overlying sediments may take place at temperatures of 800–1000°C and pressures of 10–20 kbar. These conditions can be satisfied during the subduction of a young slab (age <20 Ma) and ridge subduction initiation (Defant & Drummond, 1990; Peacock, 1990; Sajona *et al.*, 1993, 1996; Peacock *et al.*, 1994). The existence of high temperatures in the mantle wedge (Insergueix-Filippi *et al.*, 2000) induces melting of the leading edge of the slab and mantle wedge. It is possible in such an environment to attain temperatures in excess of 800°C within a relatively short time span.

The fore-arc stratigraphy observed in the Izu–Bonin and Mariana arcs provides examples in which the full geochemical record of subduction initiation and the subsequent evolution of arc magmatism is present (Ishizuka *et al.*, 2011). The evolution of these systems starts with the generation of oceanic crust, followed by the formation of fore-arc basalts, boninites, high-Mg andesites and arc andesites. The progression from subduction initiation to the establishment of normal arc volcanism lasts for no more than 7 Myr (Ishizuka *et al.*, 2011). The age distribution of igneous formations correlates with progressive LILE enrichment, from MORB-like to more enriched arc-like compositions. This development is interpreted to reflect initial decompression melting of the mantle that changed to flux melting, giving rise to high-Mg andesites, boninites and finally 'normal' arc magmatism.

A similar age distribution of igneous rocks and progressive LILE enrichment can be recognized in the Demir Kapija ophiolite. Here, the gabbros, sheeted dyke diabases and pillow basalts characterize the oceanic crust that formed in a short-lived spreading centre. Subduction-related volcanism started soon after the generation of the oceanic crust (this study; Zachariadis, 2007). The compositions of the Demir Kapija subduction-related volcanic rocks lie between those of classical adakites and typical arc magmas. Similar rocks, recognized as 'transitional adakites' or 'high-Mg andesites' (e.g. Aleutian arc; Yogodzinski & Kelemen, 1998, 2007) have been documented from the Luzon arc and the Batan and Negros Islands in the Philippines (Sajona *et al.*, 2000).

Figure 13 schematically shows a two-step petrogenetic model for the origin of the Demir Kapija subduction-related intrusions. During the initial stages of subduction, the leading edge of the slab (mafic crust + sediments) melts at lower temperatures (and pressures) in the amphibolite stability field. The parental magmas of the lavas without adakitic affinity formed during this early stage, when the depth of melting was shallower than the garnet stability field (Fig. 13a, 1). These magmas ponded at Moho depths and started to crystallize and fractionate (Fig. 13a, 2). The young Demir Kapija arc underwent a stage when the lower crust approached the amphibole-saturated solidus at 850–950°C (Smith *et al.*, 2003). This fertile crust may have been melted either by transfer of extensional strain into the crust or simply as a result of a new magma pulse (Smith *et al.*, 2003), giving rise to high-silica melts. In other words, upon and during intrusion, the replenishing melt (without adakitic affinity) is able to initiate melting of the fertile arc crust, assimilating it, and mixing

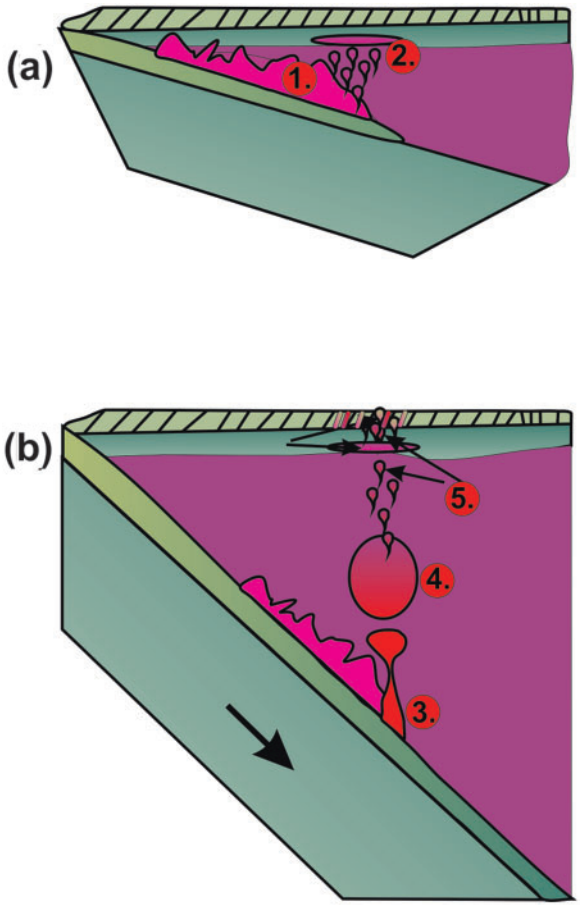

Fig. 13. Petrogenetic model for the origin of subduction-related magmas during Demir Kapija subduction initiation. The dip of the slab and its change are not to scale. (a) 1, A mixture of oceanic crust + sediments represents the melting source for the lavas without adakitic affinity, when the depth of the melting is shallower than the garnet stability field. 2, Lavas without adakitic affinity pond at Moho depths and start to crystallize and differentiate. (b) 3, Extensive melting of the oceanic crust + sediment mixture causes melting-out of plagioclase and amphibole, resulting in an apparent eclogite-like residual mineralogy in the subducted slab. This results in the generation of proto-adakitic melts. 4, The proto-adakitic melt reacts with the mantle wedge. 5, The intrusion of proto-adakitic melt into an already fractionated magma without adakitic affinity resulting in mixing and mingling. (See text for detailed discussion.)

with portions of the resident silicic magma. As subduction proceeded, melting within the slab occurred within the garnet-amphibolite stability field, giving rise to the lavas with adakitic affinity (Fig. 13b). Extensive melting caused melting-out of plagioclase and amphibole, resulting in an apparent eclogite-like residual mineralogy in the slab, which could account for the proto-adakitic features, recorded by the clinopyroxene phenocrysts (Fig. 13b, 3). The amount of sediment in the melt increases, eventually leading to increased Th contents and less radiogenic Nd isotope compositions in the rocks with adakitic affinity. Unusually high amounts of sediment input and the very unradiogenic $^{143}Nd/^{144}Nd$ seen in the rocks with adakitic affinity are a result of the proximity of continental blocks (Pelagonides and Serbian–Macedonian Massif) to the actual arc. The proto-adakitic melt, which originated by slab + sediment melting, subsequently reacted with the mantle wedge (Fig. 13b, 4); this interaction raised the Mg# and Cr and Ni content of the slab-derived melts without significantly changing their incompatible trace element ratios (Rapp *et al.*, 1999). The magmas with adakitic affinity intruded already fractionated portions of magmas without adakitic affinity, resulting in mixing and mingling (Fig. 13b, 5). This magma mixing is recorded in the clinopyroxene phenocrysts reflecting intrusion of different magma types.

In summary, the Demir Kapija oceanic basin transformed soon after rifting into an arc environment. The geochemical differences between different subduction-related lavas are interpreted to be the result of differing residual source mineralogy. This progressive change from melting of 'amphibolite' across 'garnet amphibolite' to 'eclogite' may indicate an increase in temperature within the subducted slab material soon after subduction initiation. Therefore, coexistence of melts without and with an adakitic geochemical signature may be the geochemical expression of the rapid deepening and heating of the slab.

Implications for the evolution of Tethys in the Eastern Mediterranean

The development of the Vardar Zone has been related to the Triassic opening of the Tethys ocean by continental rifting along older structural lineaments (Pe-Piper, 1998). Within the Balkan Peninsula, magmatism within these early basin and range structures was dominated by widespread sub-alkaline to alkaline and shoshonitic compositions (Robertson *et al.*, 1991; Pe-Piper, 1998; Knežević & Cvetković, 2000; Karamata, 2006). The major phase of rifting is constrained to be during the early to middle Triassic (Robertson *et al.*, 1991; Karamata, 2006) and led to the opening of an oceanic basin between Pelagonia–Drina Ivanjica and the Serbo-Macedonian Massif (Saccani *et al.*, 2003; Saccani & Photiades, 2005) named Meliata (Fig. 14a). This oceanic basin corresponds to the Vardar Zone Western Belt *sensu* Karamata (2006) or to the Eastern Vardar *sensu* Schmid *et al.* (2008).

The formation of the Demir Kapija–Guevgelia back-arc oceanic basin was probably induced by slab roll-back behind an island arc system (Fig. 14b) (Zachariadis, 2007). This arc, named the Paikon arc (Brown & Robertson, 2003, 2004), formed during the mid-Jurassic (Zachariadis, 2007). The Paikon arc is not observed in Macedonia, because either its units are covered by younger sediments or the volcanic rocks were consumed during the long and intense collisional geodynamic history.

The Paikon arc is considered to be a short-lived feature, which soon after its formation was influenced by slab roll-back that initiated spreading behind the arc and led to

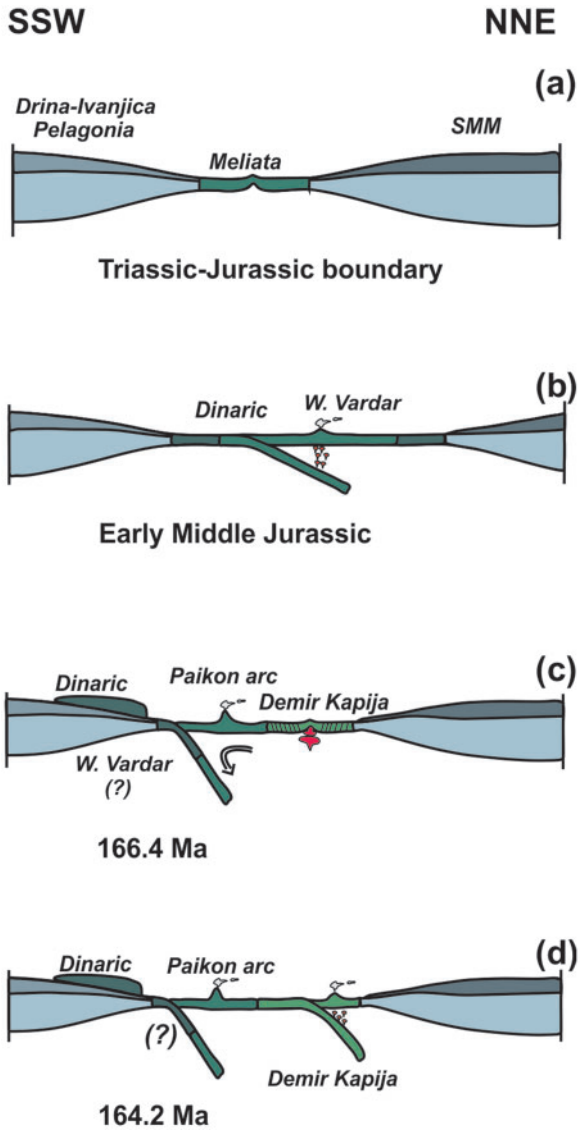

Fig. 14. Schematic cross-sections showing the plate-tectonic evolution in the Eastern Vardar system. (See text for detailed discussion.) SMM, Serbo-Macedonian Massif.

the formation of the oceanic crust preserved in the Demir Kapija–Guevgelia ophiolite complexes (Fig. 14c) (Zachariadis, 2007). The sheeted dyke diabases and pillow basalts have geochemical compositions typical of back-arc volcanic rocks originating within a short-lived spreading centre. The extensional tectonic regime changed to a compressional one associated with subduction-related volcanism within a short time span, as indicated by the narrow age range encompassed by the back-arc gabbros and plagiogranites (166 Ma; this study, Zachariadis, 2007) and the arc intrusions of Demir Kapija (164 Ma; this study; Anders *et al.*, 2005).

Subduction was initiated as a result of ridge collapse (Fig. 14d), a model previously proposed for the formation of Hellenide–Dinaride ophiolites (Spray *et al.*, 1984; Bébien *et al.*, 2000; Barth *et al.*, 2008; Barth & Gluhak, 2009). Ridge collapse is the direct result of subduction at or near a mid-ocean ridge (Boudier *et al.*, 1988). A similar model involving subduction initiation, but within older oceanic lithosphere, has been proposed for the Troodos ophiolite (Pearce & Robinson, 2010). The geochemistry of rhyolitic rocks from the Demir Kapija ophiolite requires melting of an ocean-crust source to account for the high silica contents and the small range of radiogenic $^{143}Nd/^{144}Nd$ values. Obviously, this crust needs to have high $\varepsilon Nd > +5$, which is considerably more radiogenic than the continental crust of the Serbian–Macedonian Massif and the post-collisional granites that occur within it (Fig. 8b). The terrigeneous component recognized in the entire suite of subduction-related intrusions is derived from partially melted subducted sediments that were shed from the continental Serbian–Macedonian Massif into the trench. The Demir Kapija arc volcanism and boninite magmatism within the Hellenide–Dinaride ophiolites (Barth & Gluhak, 2009) are contemporaneous with the major change in plate motion in the central Mediterranean at *c.* 165 Ma (Smith, 2006) suggesting that the two events are linked.

ACKNOWLEDGEMENTS

Ian Smith, Hugh Rollinson and an anonymous reviewer are thanked for their careful and constructive reviews, which considerably improved the clarity of the presentation and argumentation. Editorial handling by Richard Price helped to refine the final form of the paper. We acknowledge Marjorie Wilson for her tremendously diligent editorial work. We would like to thank Nora Groschopf for her assistance with XRF and microprobe analysis at the Johannes Gutenberg University of Mainz. Cüneyt Akal is acknowledged for his extremely important assistance with zircon separation. Antonis Christofides is kindly thanked for providing us with geological maps of Greece. Alistair Robertson is thanked for fruitful discussions. The paper was improved through discussions with Steve Foley.

FUNDING

This work was supported through the Deutsche Forschungsgemeinschaft (DFG) within the project BA 3441/1 and 2 and Geocycles University of Mainz Project.

SUPPLEMENTARY DATA

Supplementary data for this paper are available at *Journal of Petrology* online.

REFERENCES

Almeev, R., Holtz, F., Koepke, J., Haase, K. & Devey, C. (2008). Depths of partial crystallization of H_2O-bearing MORB: phase equilibria simulations of basalts at the MAR near Ascension Island (7–11°S). *Journal of Petrology* **49**, 25–45.

Anders, B., Reischmann, T., Poller, U. & Kostopoulos, D. (2005). Age and origin of granitic rocks of the eastern Vardar Zone, Greece: new constraints on the evolution of the Internal Hellenides. *Journal of the Geological Society, London* **162**, 857–870.

Anders, B., Reischmann, T., Kostopolous, D. & Poller, U. (2006). The oldest rocks of Greece: first evidence for a Precambrian terrane within the Pelagonian Zone. *Geological Magazine* **143**, 41–58.

Armstrong, J. T. (1995). A package of correction programs for the quantitative electron microbeam analysis of thick polished sections, thin films and particles. *Microbeam Analysis* **4**, 177–200.

Bach, W., Alt, J. C., Niu, Y., Humphris, S. E., Erzinger, J. & Dick, H. J. B. (2001). The geochemical consequences of late-stage low-grade alteration of lower ocean crust at the SW Indian Ridge: results from ODP Hole 735B (Leg 176). *Geochimica et Cosmochimica Acta* **65**, 3267–3287.

Balogh, K., Svingor, E. & Cvetković, V. (1994). Ages and intensities of metamorphic processes in the Batocina area, Serbo-Macedonian Massif. *Acta Mineralogica–Petrographica* **35**, 81–94.

Barth, M. & Gluhak, T. (2009). Geochemistry and tectonic setting of mafic rocks from the Othris Ophiolite, Greece. *Contributions to Mineralogy and Petrology* **157**, 23–40.

Barth, M., Mason, P. R. D., Davies, G. R. & Drury, M. R. (2008). The Othris Ophiolite, Greece: A snapshot of subduction initiation at a mid-ocean ridge. *Lithos* **100**, 234–254.

Beard, J. S. & Lofgren, G. E. (1991). Dehydration melting and water-saturated melting of basaltic and andesitic greenstones and amphibolites at 1, 3, and 6·9 kb. *Journal of Petrology* **32**, 365–401.

Bébien, J., Dimo-Lahitte, A., Vergeli, P., Insergueix-Filippi, D. & Dupeyrat, L. (2000). Albanian ophiolites: I. Magmatic and metamorphic processes associated with the initiation of a subduction. *Ofiolit* **25**, 39–45.

Boev, B. & Lepitkova, S. (2002). The age of the ophiolite rocks on the territory of the Republic of Macedonia. *Proceedings of XVII. Congress of Carpathian-Balkan Geological Association*, Bratislava, September, 1, 4pp. Available from: http://eprints.ugd.edu.mk/id/eprint/1430 (last accessed April 2013).

Bortolotti, V. & Principi, G. (2005). Tethyan ophiolites and Pangea break-up. *Island Arc* **14**, 442–470.

Boudier, F., Ceuleneer, G. & Nicolas, A. (1988). Shear zones, thrusts and related magmatism in the Oman ophiolite: Initiation of thrusting on an oceanic ridge. *Tectonophysics* **151**, 275–296.

Brown, S. A. M. & Robertson, A. H. F. (2003). Sedimentary geology as a key to understanding the tectonic evolution of the Mesozoic–Early Tertiary Paikon Massif, Vardar suture zone, N Greece. *Sedimentary Geology* **160**, 179–212.

Brown, S. A. M. & Robertson, A. H. F. (2004). Evidence for Neotethys rooted within the Vardar suture zone from the Voras Massif, northernmost Greece. *Tectonophysics* **381**, 143–173.

Calmus, T., Aguillón-Robles, A., Maury, R. C., Bellon, H., Benoit, M., Cotten, J., Bourgois, J. & Michaud, F. (2003). Spatial and temporal evolution of basalts and magnesian andesites ('bajaites') from Baja California, Mexico: the role of slab melts. *Lithos* **66**, 77–105.

Castillo, P. R., Janney, P. E. & Solidum, R. U. (1999). Petrology and geochemistry of Camiguin Island, southern Philippines: insights to the source of adakites and other lavas in a complex arc setting. *Contributions to Mineralogy and Petrology* **134**, 33–51.

Christofides, G., Soldatos, T. & Koroneos, A. (1990). Geochemistry and evolution of the Fanos granite, N. Greece. *Mineralogy and Petrology* **43**, 49–63.

Crawford, A. J., Falloon, T. J. & Green, D. H. (1989). Classification, petrogenesis and tectonic setting of boninites. In: Crawford, A. J. (ed.) *Boninites and Related Rocks*. London: Unwin Hyman, pp. 1–49.

Dalrymple, G. B. & Duffield, W. A. (1988). High precision $^{40}Ar/^{39}Ar$ dating of Oligocene rhyolites from the Mogollon–Datil volcanic field using a continuous laser system. *Geophysical Research Letters* **15**, 463–466.

Deer, W. A., Howie, R. A. & Zussman, J. (1992). *An Introduction to the Rock-forming Minerals*, 2nd edn. Harlow: Longman.

Defant, M. J. & Drummond, M. S. (1990). Derivation of some modern arc magmas by melting of young subducted lithosphere. *Nature* **347**, 662–665.

Falloon, T. J., Danyushevsky, L. V., Crawford, A. J., Meffre, S., Woodhead, J. D. & Bloomer, S. H. (2008). Boninites and adakites from the northern termination of the Tonga Trench: implications for adakite petrogenesis. *Journal of Petrology* **49**, 697–715.

Gaetani, G. A. & Grove, T. L. (1995). Partitioning of rare earth elements between clinopyroxene and silicate melt: Crystal-chemical controls. *Geochimica et Cosmochimica Acta* **59**, 1951–1962.

Green, T. H. & Pearson, N. J. (1986). Ti-rich accessory phase saturation in hydrous mafic–felsic compositions at high *P*, *T*. *Chemical Geology* **54**, 185–201.

Grove, T. L., Kinzler, R. J. & Bryan, W. B. (1992). Fractionation of midocean ridge basalt (MORB). In: Phipps Morgan, J., Blackman, D. K. & Sinton, J. M. (eds) *Mantle Flow and Melt Generation at Mid-Ocean Ridges. American Geophysical Union, Geophysical Monograph* **152**, 281–310.

Hart, S. R., Blusztajn, J., Dick, H. J. B., Meyer, P. S. & Muehlenbachs, K. (1999). The fingerprint of seawater circulation in a 500-meter section of ocean crust gabbros. *Geochimica et Cosmochimica Acta* **63**, 4059–4080.

Hawkesworth, C. J., Turner, S. P., McDermott, F., Peate, D. W. & van Calsteren, P. (1997). U–Th isotopes in arc magmas: implications for element transfer from the subducted crust. *Science* **276**, 551–555.

Hermann, J. & Spandler, C. J. (2008). Sediment melts at sub-arc depths: an experimental study. *Journal of Petrology* **49**, 717–740.

Himmerkus, F., Reischmann, T. & Kostopoulos, D. (2002). First evidence for Silurian magmatism in the Serbo-Macedonian Massif, northern Greece. *Geochimica et Cosmochimica Acta* **66**, A330–A330.

Himmerkus, F., Reischmann, T. & Kostopoulos, D. (2009*a*). Serbo-Macedonian revisited: A Silurian basement terrane from northern Gondwana in the Internal Hellenides, Greece. *Tectonophysics* **473**, 20–35.

Himmerkus, F., Reischmann, T. & Kostopoulos, D. (2009*b*). Triassic rift-related meta-granites in the Internal Hellenides, Greece. *Geological Magazine* **146**, 252–265.

Insergueix-Filippi, D., Dupeyrat, L., Dimo-Lahitte, A., Vergely, P. & Bébien, J. (2000). Albanian ophiolites. II—model of subduction zone infancy at a mid-ocean ridge. *Ofioliti* **25**, 47–53.

Ishikawa, T., Fujisawa, S., Nagaishi, K. & Masuda, T. (2005). Trace element characteristics of the fluid liberated from amphibolite-facies slab: Inference from the metamorphic sole beneath the Oman ophiolite and implication for boninite genesis. *Earth and Planetary Science Letters* **240**, 355–377.

Ishizuka, O., Yuasa, M., Tamura, Y., Shukuno, H., Stern, R. J., Naka, J., Joshima, M. & Taylor, R. N. (2010). Migrating shoshonitic magmatism tracks Izu–Bonin–Mariana intra-oceanic arc rift propagation. *Earth and Planetary Science Letters* **294**, 111–122.

Ishizuka, O., Tani, K., Reagan, M. K., Kanayama, K., Umino, S., Harigane, Y., Sakamoto, I., Miyajima, Y., Yuasa, M. & Dunkley, D. J. (2011). The timescales of subduction initiation and subsequent evolution of an oceanic island arc. *Earth and Planetary Science Letters* **306**, 229–240.

Jackson, S. E., Pearson, N. J., Griffin, W. L. & Belousova, E. A. (2004). The application of laser ablation-inductively coupled plasma mass spectrometry to *in situ* U–Pb zircon geochronology. *Chemical Geology* **211**, 47–69.

Jochum, K. D., Weis, U., Stoll, B., Kuzmin, D., Yang, Q., Raczek, I., Jacob, D. E., Stracke, A., Birbaum, K., Frick, D. A., Günther, D. & Enzweiler, J. (2011). Determination of reference values for NIST SRM 610–617 glasses following ISO guidelines. *Geostandards and Geoanalytical Research* **35**, 397–429.

Johnson, K. T. M. (1998). Experimental determination of partition coefficients for rare earth and high-field-strength elements between clinopyroxene, garnet, and basaltic melt at high pressures. *Contributions to Mineralogy and Petrology* **133**, 60–68.

Johnson, M. C. & Plank, T. (1999). Dehydration and melting experiments constrain the fate of subducted sediments. *Geochemistry, Geophysics, Geosystems* **1(12)**, 1007, doi:10.1029/1999GC000014.

Johnson, T. E., Fischer, S., White, R. W., Brown, M. & Rollinson, H. R. (2012). Intracrustal differentiation from partial melting of metagabbro—field and geochemical evidence from the central region of the Neoarchaean Lewisian Complex, NW Scotland. *Journal of Petrology* **53**, 2115–2138.

Karamata, S. (2006). The geological development of the Balkan Peninsula related to the approach, collision and compression of Gondwanan and Eurasian units. In: Robertson, A. H. F. & Mountrakis, D. (eds) *Tectonic Development of the Eastern Mediterranean Region. Geological Society, London, Special Publications* **260**, 155–178.

Knežević, V. & Cvetković, V. (2000). Triassic rifting magmatism of the Dinarides. In: Karamata, S. & Jankovic, S. (eds) *Proceedings of the International Symposium 'Geology and Metallogeny of the Dinarides and the Vardar Zone'. Academy of Science and Arts of the Republic of Srpska, Collections and Monographs* **1**, 149–160.

Koepke, J., Feig, S., Snow, J. & Freise, M. (2004). Petrogenesis of oceanic plagiogranites by partial melting of gabbros: an experimental study. *Contributions to Mineralogy and Petrology* **146**, 414–432.

Koepke, J., Berndt, J., Feig, S. & Holtz, F. (2007). The formation of SiO_2-rich melts within the deep oceanic crust by hydrous partial melting of gabbros. *Contributions to Mineralogy and Petrology* **153**, 67–84.

Le Bas, M. J., Le Maitre, R. W., Streckeisen, A. & Zanettin, B. A. (1986). Chemical classification of volcanic rocks based on the total alkali–silica diagram. *Journal of Petrology* **27**, 745–750.

Lepitkova, S. (2002). Petroloski, geohemijski i izotopski proucuvanja na peridotitite od vnatresniot dinarski ofiolitski pojas vo Republika Makedonija. PhD dissertation, Kiril and Metodij University of Skopje, 333 pp.

Ludwig, K. R. (2003). *User's Manual for Isoplot 3.0. Berkeley Geochronology Center. Special Publication* **4**, .

Macpherson, C. G., Dreher, S. T. & Thirlwall, M. F. (2006). Adakites without slab melting: High pressure differentiation of island arc magma, Mindanao, the Philippines. *Earth and Planetary Science Letters* **243**, 581–593.

Marović, M., Djoković, I., Pešić, L., Toljić, M. & Gerzina, N. (2000). The genesis and geodynamics of Cenozoic sedimentation provinces of the central Balkan Peninsula. *Geotectonics* **34**, 415–427.

Martin, H. (1999). Adakitic magmas: modern analogues of Archaean granitoids. *Lithos* **46**, 411–429.

Martin, H., Smithies, R. H., Rapp, R., Moyen, J. F. & Champion, D. (2005). An overview of adakite, tonalite–trondhjemite–granodiorite (TTG), and sanukitoid: relationships and some implications for crustal evolution. *Lithos* **79**, 1–24.

Meinhold, G., Kostopoulos, D., Frei, D., Himmerkus, F. & Reischmann, T. (2010). U–Pb LA-SF-ICP-MS zircon geochronology of the Serbo-Macedonian Massif, Greece: palaeotectonic constraints for Gondwana-derived terranes in the Eastern Mediterranean. *International Journal of Earth Sciences* **99**, 813–832.

Miyashiro, A. (1975). Volcanic rock series and tectonic setting. *Annual Review of Earth and Planetary Sciences* **3**, 251–269.

Nehring, F., Jacob, D. E., Barth, M. G. & Foley, S. F. (2008). Laser-ablation ICP-MS analysis of siliceous rock glasses fused on an iridium strip heater using MgO dilution. *Microchimica Acta* **160**, 153–163.

Pamić, J., Tomljenović, B. & Balen, D. (2002). Geodynamic and petrogenetic evolution of Alpine ophiolites from the central and NW Dinarides: an overview. *Lithos* **65**, 113–142.

Patino, L. C., Carr, M. J. & Feigenson, M. D. (2000). Local and regional variations in Central American arc lavas controlled by variations in subducted sediment input. *Contributions to Mineralogy and Petrology* **138**, 265–283.

Peacock, S. A. (1990). Fluid processes in subduction zones. *Science* **248**, 329–337.

Peacock, S. M., Rushmer, T. & Thompson, A. B. (1994). Partial melting of subducting oceanic crust. *Earth and Planetary Science Letters* **121**, 227–244.

Pearce, J. A. & Cann, J. R. (1973). Tectonic setting of basic volcanic rocks determined using trace element analyses. *Earth and Planetary Science Letters* **19**, 290–300.

Pearce, J. A. & Peate, D. W. (1995). Tectonic implications of the composition of volcanic arc magmas. *Annual Review of Earth and Planetary Sciences* **23**, 251–285.

Pearce, J. A. & Robinson, P. T. (2010). The Troodos ophiolitic complex probably formed in a subduction initiation, slab edge setting. *Gondwana Research* **18**, 60–81.

Pearce, J. A. & Stern, R. J. (2006). The origin of back-arc basin magmas: trace element and isotope perspectives. In: Christie, D. M., Fisher, C. R., Lee, S.-M. & Givens, S. (eds) *Back-arc Spreading Systems: Geological, Biological, Chemical and Physical Interactions. American Geophysical Union, Geophysical Monograph* **166**, 63–86.

Pearce, J. A., Lippard, S. J. & Roberts, S. (1984). Characteristics and tectonic significance of supra-subduction zone ophiolites. In: Kokelaar, B. P. & Howells, M. F. (eds) *Marginal Basin Geology: Volcanic and Associated Sedimentary and Tectonic Processes in Modern and Ancient Marginal Basins. Geological Society, London, Special Publications* **16**, 77–94.

Peccerillo, A. & Taylor, S. R. (1976). Geochemistry of Eocene calc-alkaline volcanic rocks from the Kastamonu area, Northern Turkey. *Contributions to Mineralogy and Petrology* **58**, 63–81.

Pe-Piper, G. (1998). The nature of Triassic extension-related magmatism in Greece: evidence from Nd and Pb isotope geochemistry. *Geological Magazine* **135**, 331–348.

Plank, T. (2005). Constraints from thorium/lanthanum on sediment recycling at subduction zones and the evolution of the continents. *Journal of Petrology* **46**, 921–944.

Prelević, D., Foley, S. F., Romer, R. & Conticelli, S. (2008). Mediterranean Tertiary lamproites derived from multiple source components in postcollisional geodynamics. *Geochimica et Cosmochimica Acta* **72**, 2125–2156.

Rapp, R. P. & Watson, E. B. (1995). Dehydration melting of metabasalt at 8–32 kbar: implications for continental growth and crust–mantle recycling. *Journal of Petrology* **36**, 891–931.

Rapp, R. P., Watson, E. B. & Miller, C. F. (1991). Partial melting of amphibolite/eclogite and the origin of Archean trondhjemites and tonalites. *Precambrian Research* **51**, 1–25.

Rapp, R. P., Shimizu, N., Norman, M. D. & Applegate, G. S. (1999). Reaction between slab-derived melts and peridotite in the mantle wedge: experimental constraints at 3·8 GPa. *Chemical Geology* **160**, 335–356.

Rapp, R. P., Irifune, T., Shimizu, N., Nishiyama, N., Norman, M. D. & Inoue, T. (2008). Subduction recycling of continental sediments and the origin of geochemically enriched reservoirs in the deep mantle. *Earth and Planetary Science Letters* **271**, 14–23.

Reagan, M. K., Ishizuka, O., Stern, R. J., Kelley, K. A., Ohara, Y., Blichert-Toft, J., Bloomer, S. H., Cash, J., Fryer, P., Hanan, B. B., Hickey-Vargas, R., Ishii, T., Kimura, J.-I., Peate, D. W., Rowe, M. C. & Woods, M. (2010). Fore-arc basalts and subduction initiation in the Izu–Bonin–Mariana system. *Geochemistry, Geophysics, Geosystems* **11**, Q03X12, doi:10.1029/2009gc002871.

Robertson, A., Karamata, S. & Šarić, K. (2009). Overview of ophiolites and related units in the Late Palaeozoic–Early Cenozoic magmatic and tectonic development of Tethys in the northern part of the Balkan region. *Lithos* **108**, 1–36.

Robertson, A. H. F., Clift, P. D., Degnan, P. J. & Jones, G. (1991). Palaeogeographic and palaeotectonic evolution of the Eastern Mediterranean Neotethys. *Palaeogeography, Palaeoclimatology, Palaeoecology* **87**, 289–343.

Rogers, G., Saunders, A. D., Terrell, D. J., Verma, S. P. & Marriner, G. F. (1985). Geochemistry of Holocene volcanic rocks associated with ridge subduction in Baja California, Mexico. *Nature* **315**, 389–392.

Rollinson, H. (2009). New models for the genesis of plagiogranites in the Oman ophiolite. *Lithos* **112**, 603–614.

Romer, R. L., Foerster, H. J. & Breitkreuz, C. (2001). Intracontinental extensional magmatism with a subduction fingerprint; the Late Carboniferous Halle volcanic complex (Germany). *Contributions to Mineralogy and Petrology* **141**, 201–221.

Romer, R. L., Heinrich, W., Schröder-Smeibidl, B., Meixner, A., Fischer, C.-O. & Schulz, C. (2005). Elemental dispersion and stable isotope fractionation during reactive fluid-flow and fluid immiscibility in the Bufa del Diente aureole, NE Mexico: evidence from radiographies and Li, B, Sr, Nd, and Pb isotope systematics. *Contributions to Mineralogy and Petrology* **149**, 400–429.

Ryerson, F. J. & Watson, E. B. (1987). Rutile saturation in magmas: implications for Ti–Nb–Ta depletion in island-arc basalts. *Earth and Planetary Science Letters* **86**, 225–239.

Saccani, E. & Photiades, A. (2005). Petrogenesis and tectonomagmatic significance of volcanic and subvolcanic rocks in the Albanide–Hellenide ophiolitic mélanges. *Island Arc* **14**, 494–516.

Saccani, E., Padoa, E. & Photiades, A. (2003). Triassic mid-ocean ridge basalts from the Argolis Peninsula (Greece): new constraints for the early oceanization phases of the Neo-Tethyan Pindos basin. In: Dilek, Y. & Robinson, P. T. (eds) *Ophiolites in Earth History. Geological Society, London, Special Publications* **218**, 109–127.

Saccani, E., Beccaluva, L., Photiades, A. & Zeda, O. (2011). Petrogenesis and tectono-magmatic significance of basalts and mantle peridotites from the Albanian–Greek ophiolites and sub-ophiolitic mélanges. New constraints for the Triassic–Jurassic evolution of the Neo-Tethys in the Dinaride sector. *Lithos* **124**, 227–242.

Sadofsky, S., Portnyagin, M., Hoernle, K. & van den Bogaard, P. (2008). Subduction cycling of volatiles and trace elements through the Central American volcanic arc: evidence from melt inclusions. *Contributions to Mineralogy and Petrology* **155**, 433–456.

Sajona, F. G., Maury, R. C., Bellon, H., Cotten, J., Defant, M. J. & Pubellier, M. (1993). Initiation of subduction and the generation of slab melts in western and eastern Mindanao, Philippines. *Geology* **21**, 1007–1010.

Sajona, F. G., Maury, R. C., Bellon, H., Cotten, J. & Defant, M. (1996). High field strength element enrichment of Pliocene–Pleistocene island arc basalts, Zamboanga Peninsula, Western Mindanao (Philippines). *Journal of Petrology* **37**, 693–726.

Sajona, F. G., Maury, R. C., Prouteau, G., Cotten, J., Schiano, P., Bellon, H. & Fontaine, L. (2000). Slab melt as metasomatic agent in island arc magma mantle sources, Negros and Batan (Philippines). *Island Arc* **9**, 472–486.

Šarić, K., Cvetković, V., Romer, R. L., Christofides, G. & Koroneos, A. (2009). Granitoids associated with East Vardar ophiolites (Serbia, F.Y.R. of Macedonia and northern Greece): Origin, evolution and geodynamic significance inferred from major and trace element data and Sr–Nd–Pb isotopes. *Lithos* **108**, 131–150.

Schmid, S., Bernoulli, D., Fügenschuh, B., Matenco, L., Schefer, S., Schuster, R., Tischler, M. & Ustaszewski, K. (2008). The Alpine–Carpathian–Dinaridic orogenic system: correlation and evolution of tectonic units. *Swiss Journal of Geosciences* **101**, 139–183.

Sen, C. & Dunn, T. (1994). Dehydration melting of a basaltic composition amphibolite at 1·5 and 2·0 GPa: implications for the origin of adakites. *Contributions to Mineralogy and Petrology* **117**, 394–409.

Shervais, J. W. (1982). Ti–V plots and the petrogenesis of modern and ophiolitic lavas. *Earth and Planetary Science Letters* **59**, 101–118.

Slama, J., Kosler, J., Condon, D. J., Crowley, J. L., Gerdes, A., Hanchar, J. M., Horstwood, M. S. A., Morris, G. A., Nasdala, L., Norberg, N., Schaltegger, U., Schoene, B., Tubrett, M. N. & Whitehouse, M. J. (2008). Plesovice zircon—A new natural reference material for U–Pb and Hf isotopic microanalysis. *Chemical Geology* **249**, 1–35.

Smith, A. G. (2006). Tethyan ophiolite emplacement, Africa to Europe motions and Atlantic spreading. In: Robertson, A. H. F. & Mountrakis, D. (eds) *Tectonic Development of the Eastern Mediterranean Region. Geological Society, London, Special Publications* **260**, 11–34.

Smith, I. E. M., Worthington, T. J., Stewart, R. B., Price, R. C. & Gamble, J. A. (2003). Felsic volcanism in the Kermadec arc, SW Pacific: crustal recycling in an oceanic setting. In: Larter, R. D. & Leat, P. T. (eds) *Intra-Oceanic Subduction Systems: Tectonic and Magmatic Processes. Geological Society, London, Special Publications* **1**, 99–118.

Sobolev, A. V., Migdisov, A. A. & Portnyagin, M. V. (1996). Incompatible element partitioning between clinopyroxene and basalt liquid revealed by the study of melt inclusions in minerals from Troodos lavas, Cyprus. *Petrology* **4**, 307–317.

Spray, J. G., Babien, J., Rex, D. C. & Roddick, J. C. (1984). Age constraints on the igneous and metamorphic evolution of the Hellenic–Dinaric ophiolites. In: Dixon, J. E. & Robertson, A. H. F. (eds) *The Geological Evolution of the Eastern Mediterranean. Geological Society, London, Special Publications* **17**, 619–627.

Stacey, J. S. & Kramers, J. D. (1975). Approximation of terrestrial lead isotope evolution by a two-stage model. *Earth and Planetary Science Letters* **26**, 207–221.

Stern, R. J. & Bloomer, S. H. (1992). Subduction zone infancy; examples from the Eocene Izu–Bonin–Mariana and Jurassic California arcs. *Geological Society of America Bulletin* **104**, 1621–1636.

Sun, S. S. & McDonough, W. F. (1989). Chemical and isotopic systematics of oceanic basalts; implications for mantle composition and processes. In: Saunders, A. D. & Norry, M. J. (eds) *Magmatism in the Ocean Basins. Geological Society, London, Special Publications* **42**, 313–345.

Tiepolo, M., Oberti, R., Zanetti, A., Vannucci, R. & Foley, S. F. (2007). Trace-element partitioning between amphibole and silicate melt. In: Hawthorne, F. C., Oberti, R., Della Ventura, G. &

Mottana, A. (eds) *Amphiboles: Crystal Chemistry, Occurrence and Health Issues. Mineralogical Society of America and Geochemical Society, Reviews in Mineralogy and Geochemistry* **67**, 417–452.

Ustaszewski, K., Schmid, S. M., Lugovic, B. K., Schuster, R., Schaltegger, U., Bernoulli, D., Hottinger, L., Kounov, A., Fügenschuh, B. & Schefer, S. (2009). Late Cretaceous intra-oceanic magmatism in the internal Dinarides (northern Bosnia and Herzegovina): Implications for the collision of the Adriatic and European plates. *Lithos* **108**, 106–125.

Van Achterbergh, E., Ryan, C. G., Jackson, S. E. & Griffin, W. L. (2000). Data reduction software for LA-ICPMS: Appendix. In: Sylvester, P. J. (ed.) *Laser Ablation-ICP-Mass Spectrometry in the Earth Sciences: Principles and Applications. Mineralogical Association of Canada, Short Course Series* **40**, 239–243.

Van den Bogaard, P. (1995). $^{40}Ar/^{39}Ar$ ages of sanidine phenocrysts from Laacher See Tephra (12,900 yr BP): Chronostratigraphic and petrological significance. *Earth and Planetary Science Letters* **133**, 163–174.

Whattam, S. & Stern, R. (2011). The 'subduction initiation rule': a key for linking ophiolites, intra-oceanic forearcs, and subduction initiation. *Contributions to Mineralogy and Petrology* **162**, 1031–1045.

Wiedenbeck, M., Allé, P., Corfu, F., Griffin, W. L., Meier, M., Oberli, F., von Quadt, A., Roddick, J. C. & Spiegel, W. (1995). Three natural zircon standards for U–Th–Pb, Lu–Hf, trace element and REE analyses. *Geostandards Newsletter* **19**, 1–23.

Winchester, J. A. & Floyd, P. A. (1977). Geochemical discrimination of different magma series and their differentiation products using immobile elements. *Chemical Geology* **20**, 325–343.

Yogodzinski, G. M. & Kelemen, P. B. (1998). Slab melting in the Aleutians: implications of an ion probe study of clinopyroxene in primitive adakite and basalt. *Earth and Planetary Science Letters* **158**, 53–65.

Yogodzinski, G. M. & Kelemen, P. B. (2007). Trace elements in clinopyroxenes from Aleutian xenoliths: Implications for primitive subduction magmatism in an island arc. *Earth and Planetary Science Letters* **256**, 617–632.

Zachariadis, P. (2007). Ophiolites of the eastern Vardar Zone, N. Greece. PhD dissertationMainz: Johannes Gutenberg-Universität, 131 p.

Zelić, M., Marroni, M., Pandolfi, L. & Trivic, B. (2010). Tectonic setting of the Vardar suture zone (Dinaric–Hellenic belt): The example of the Kopaonik area (Southern Serbia). *Ofioliti* **35**, 49–69.

Zhang, S. Q., Mahoney, J. J., Mo, X. X., Ghazi, A. M., Milani, L., Crawford, A. J., Guo, T. Y. & Zhao, Z. D. (2005). Evidence for a widespread Tethyan upper mantle with Indian-Ocean-type isotopic characteristics. *Journal of Petrology* **46**, 829–858.